

AD-A119 798

NORWEGIAN DEFENCE RESEARCH ESTABLISHMENT KJELLER
THE BEHAVIOUR OF AL ELECTRODES IN AQUEOUS SOLUTIONS,(U)
AUG 81 T VALAND
NDRE/PUBL-81/1003

F/G 7/4

UNCLASSIFIED

NL

1 OF 1
AD A
18798

END
DATE
FILMED
1982
DTIC

①

THE BEHAVIOUR OF AI ELECTRODES IN AQUEOUS SOLUTIONS

BY

TORSTEIN VÅLAND

NDRE/PUBL-81/1003
ISSN 0085-4301

DTIC
ELECTE
S OCT 1 1982
A

This document has been approved
for public release and sale; its
distribution is unlimited.

FORSVARETS FORSKNING SINSTITUTT
NORWEGIAN DEFENCE RESEARCH ESTABLISHMENT
P O Box 25 - N-2007 Kjeller, Norway

82 10 01 012

AD A119798

DTIC FILE COPY

THE BEHAVIOUR OF AI ELECTRODES IN AQUEOUS SOLUTIONS

by

Torstein Våland

NDRE/PUBL-81/1003

ISSN 0085-4301

FORSVARETS FORSKNING SINSTITUTT

NORWEGIAN DEFENCE RESEARCH ESTABLISHMENT


P O Box 25 - N-2007 Kjeller, Norway

August 1981

NORWEGIAN DEFENCE RESEARCH ESTABLISHMENT (NDRE)
 FORSVARETS FORSKNING SINSTITUTT (FFI)
 POST OFFICE BOX 25
 N 2007 KJELLER, NORWAY

UNCLASSIFIED
 SECURITY CLASSIFICATION OF THIS PAGE
 (when data entered)

REPORT DOCUMENTATION PAGE

1. PUBL. REPORT NUMBER NDRE/PUBL- 81/1003 2. AUTHOR REFERENCE 376 VM/159	2. SECURITY CLASSIFICATION UNCLASSIFIED 2a) DECLASSIFICATION DOWNGRADING SCHEDULE	3. NUMBER OF PAGES 83												
4. TITLE THE BEHAVIOUR OF AL ELECTRODES IN AQUEOUS SOLUTIONS														
5. NAMES OF AUTHOR(S) IN FULL (surname first) VALAND Torstein														
6. DISTRIBUTION STATEMENT Approved for public release. Distribution unlimited. (offentlig tilgjengelig)														
7. INDEXING TERMS <table border="0"> <tr> <td>IN ENGLISH</td> <td>IN NORWEGIAN</td> </tr> <tr> <td>a) Electrochemistry</td> <td>a) Elektrokjemi</td> </tr> <tr> <td>b) Passivity</td> <td>b) Passivitet</td> </tr> <tr> <td>c) Anodic coating</td> <td>c) Anodiske filmer</td> </tr> <tr> <td>d) Ionic transport properties</td> <td>d) Ione transport egenskaper</td> </tr> <tr> <td>e) Semiconductivity</td> <td>e) Halvlederegenskaper</td> </tr> </table> 7a) AUTHOR REFERENCE Thesaurus of metallurgical terms (ASM)			IN ENGLISH	IN NORWEGIAN	a) Electrochemistry	a) Elektrokjemi	b) Passivity	b) Passivitet	c) Anodic coating	c) Anodiske filmer	d) Ionic transport properties	d) Ione transport egenskaper	e) Semiconductivity	e) Halvlederegenskaper
IN ENGLISH	IN NORWEGIAN													
a) Electrochemistry	a) Elektrokjemi													
b) Passivity	b) Passivitet													
c) Anodic coating	c) Anodiske filmer													
d) Ionic transport properties	d) Ione transport egenskaper													
e) Semiconductivity	e) Halvlederegenskaper													
8. ABSTRACT (continue on reverse side if necessary) <p>In this work the behaviour of oxide covered Al electrodes in aqueous solutions is treated. Emphasis is laid on the behaviour at low electrode potentials, <i>ie</i> below approximately -1.0 V (SCE). Based on the general theories of passivation developed by K.J Vetter, a thermodynamic treatment of the electrode is reported.</p> <p>Results obtained from experiments with pure and alloyed Al are given. Usually, the potential step technique was used in these experiments, but other techniques, such as capacity measurements, were also applied. These results are discussed in the light of the thermodynamic treatment, especially when the ion transfer and the oxide formation process is considered.</p> <p>The cathodic hydrogen evolution reaction has been treated by assuming that the step involving electron transfer is rate determining. The effects of oxide thickness and alloying elements on the hydrogen evolution reaction are discussed in accordance with this assumption. In this connection, the effect of separate phases formed on the electrode surface by the alloying elements is also discussed.</p>														
9. DATE 1 August 1981	AUTHORIZED BY  P Thoresen	POSITION Superintendent												

Special attention has been paid to the presentation of present-day knowledge in the field, not only on oxide covered aluminium but also on other passive metals.

The hydrogen evolution reaction has been treated according to a model of electron transfer. A similar model was proposed by Vetter and Schultze for the oxygen evolution reaction on passive metals. The impurity effects on the electrochemical properties of the oxide covered aluminium have partly been explained by means of this model.

The author wishes to acknowledge the support of the Norwegian Defence Research Establishment. Thanks are especially due to Dr Per Thoresen for his encouragement and to Mr G Nilsson for experimental work.

[illegible]

CONTENTS

	Page
1 INTRODUCTION	9
1.1 Behaviour of Al electrodes	9
1.2 Anodic polarization	10
1.3 The porous oxide layer	10
1.4 Cathodic polarization	11
1.5 The cathodic break-down potential	12
1.6 Film thinning and hydration	13
1.7 The duplex film	15
1.8 Other metal oxide films	15
1.9 The Al electrode in aqueous solution	16
2 THERMODYNAMIC CONSIDERATIONS	17
2.1 General	17
2.2 The metal-oxide interface	18
2.3 The oxide-electrolyte interface	20
2.4 The oxide film	22
3 REACTIONS AT THE OXIDE-ELECTROLYTE INTERFACE	26
3.1 General	26
3.2 "Tafel" curves of the reactions	28
3.3 The pH dependency of the reactions	29
3.4 Stationary metal dissolution current	30
4 THE INFLUENCE OF POTENTIAL STEPS ON Al-ELECTRODES COVERED WITH THIN OXIDE FILMS	33
4.1 General	33
4.2 Ion transport	35
4.3 Electron transport	36
4.4 Electrode capacitance	38
4.5 Experimental	40
4.6 Results	41
4.7 Discussion	46
4.7.1 The steady state anodic dissolution rate at low potentials	46
4.7.2 Ion transport through the oxide	47
4.7.3 Electron transport	49
5 THE CAPACITANCE OF THE Al ELECTRODE	53
5.1 General	53
5.2 Experimental	55
5.3 Results	56
5.4 Discussion	58

		Page
6	THE INFLUENCE OF IMPURITIES ON ALUMINIUM	64
6.1	General	64
6.2	Experimental	66
6.3	Results	66
6.4	Discussion	69
7	THE PROPERTIES OF OXIDE COVERED AI - AN OVERVIEW	73
	References	76
	List of symbols	80

THE BEHAVIOUR OF Al ELECTRODES IN AQUEOUS SOLUTIONS

SUMMARY

In this work the behaviour of oxide covered Al electrodes in aqueous solutions is treated. Emphasis is laid on the behaviour at low electrode potentials, *i.e.* below approximately -1.0 V (SCE). Based on the general theories of passivation developed by K.J. Vetter, a thermodynamic treatment of the electrode is reported.

Results obtained from experiments with pure and alloyed Al are given. Usually, the potential step technique was used in these experiments, but other techniques, such as capacity measurements, were also applied. These results are discussed in the light of the thermodynamic treatment, especially when the ion transfer and the oxide formation processes are considered.

The cathodic hydrogen evolution reaction has been treated by assuming that the step involving electron transfer is rate determining. The effects of oxide thickness and alloying elements on the hydrogen evolution reaction are discussed in accordance with this assumption. In this connection, the effect of separate phases formed on the electrode surface by the alloying elements is also discussed.

1 INTRODUCTION

1.1 Behaviour of Al electrodes

When aluminium is immersed in aqueous solutions, it will acquire an open circuit potential which is more noble than the thermodynamic equilibrium potential of the active Al/Al^{3+} electrode.

If the electrode is polarized, Tafel curves can be obtained in both the anodic and cathodic direction (13,19,47,49). The curves are not stable, however, and will change with time of polarization.

The cathodic reaction is usually either the reduction of oxygen dissolved in water or the evolution of hydrogen. The anodic reaction is the oxydation of Al. The observed open circuit potential is therefore a mixed potential, as also pointed out by Kunze (47) and Kaesche (43). As such, it is highly dependent on the environment and on the experimental conditions. Usually the open circuit potential will be above -1.0 V (SCE), but when the Al is very pure, or certain small amounts of alloying elements are present, open circuit potentials below -1.5 V (SCE) can be obtained (17,63).

The large variation in the open circuit potential is probably due partly to changes in the properties of the oxide film covering the electrode. The film, which is formed in air as well as in aqueous solutions, plays an important role in determining the electrochemical properties of the Al electrode.

When the film is compact, ions and/or electrons must move through it in order to enable the electrochemical reactions to proceed at the electrode surface. The ionic and electronic conductivity and the thickness of the oxide film will therefore be main parameters in determining the potential of the electrode and the reaction rates.

If chlorides or other aggressive ions are present in the solution, the oxide film can be attacked. Heavy pitting corrosion may then be observed. Often a certain potential limit, the *pitting potential* must be exceeded for pitting to occur. For Al in chloride solutions the pitting potential is approximately -0.8 V (SCE). Pitting on Al has been described by several authors (41,42,43,55,88) and will not be dealt with further in this work.

1.2 Anodic polarization

When aggressive ions are absent, the time dependent anodic Tafel curves are seen to be displaced towards smaller current density values, *i.e.* the reaction rate at constant potential seems to become slower when an anodic current is flowing. This has clearly been demonstrated by Kunze (47). The variation is probably due to changes in the oxide film, either in thickness or in other properties.

If the electrode is highly polarized, *i.e.* from a few volts and up to several hundred volts, a compact oxide film is formed. This so-called *barrier film* will grow in thickness until a certain thickness value is reached. This value is linearly dependent upon the applied voltage. The proportionality factor (*anodizing ratio*) varies slightly, but has a value in the vicinity of 13 Å/V (30). It can be assumed that most of the voltage change in these films takes place across the oxide film. The constant anodizing ratio therefore indicates that the electric field is nearly constant across the film and equal to $\sim 7.5 \cdot 10^8$ V/m. It is independent of the thickness and virtually independent of the electrolyte composition. In some electrolytes deviation from the constant value is found. This will be treated later.

Usually the barrier film is formed by anodizing with a constant current until a certain voltage is reached. The voltage is then kept at this constant value. A current decay will then take place. Gunterschultze *et al* (26) have shown that the current density (j) is related to the anodizing voltage (E_F) by the equation

$$j = A \exp(B E_F / \delta) \quad (1.1)$$

The constants A and B have the values $3.62 \cdot 10^{-19}$ A/m² and $4.25 \cdot 10^{-8}$ m/V respectively (26). δ is the oxide thickness.

Young (94) has shown that a plot of $\log j$ vs the field strength is not strictly linear. He has therefore proposed that Equation (1.1) should be replaced by the equation

$$j = A \exp[(\alpha - \beta V)V / kT] \quad (1.2)$$

where α and β are new constants, and V is the electric field, *i.e.* usually E_F / δ . As a first approximation Equation (1.1) is, however, sufficiently accurate.

1.3 The porous oxide layer

When Al is anodized in acids like sulphuric, phosphoric or oxalic acid, the barrier layer is still formed. It is however thinner than that observed in neutral solutions.

While the anodizing ratio in neutral solutions is nearly constant, the ratio becomes dependent on both the electrolyte type and concentration when the solution is acid. In 40–60% w/w sulphuric acid Hunter *et al* (39) found the anodizing ratio to be as small as 8 Å/V while O'Sullivan *et al* (60) in 0.4 M phosphoric acid found it to be 10.4 Å/V.

Even though the barrier layer becomes thinner in acid solutions, the total film thickness may sometimes become much thicker than in neutral solutions. Upon the barrier layer, a porous layer is formed. The thickness of this layer is independent of the voltage applied but depends on the current and the time of anodization. While the barrier layer is limited to a thickness of approximately 5000 Å (14), the porous layer can become much thicker.

The formation of a porous layer can usually be seen from the voltage *vs* time curves. When the barrier layer is formed at a constant current, the voltage will increase linearly with time until the desired formation voltage is reached or an electric breakdown takes place. If, on the other hand, a porous layer is formed, the voltage *vs* time curve will deviate from a straight line. After reaching a maximum, it will decrease somewhat before the voltage becomes constant. O'Sullivan *et al* (60) have shown that the porous layer is already in evolution when the voltage maximum is reached.

1.4 Cathodic polarization

If the potential of the Al electrode is low, either because the open circuit potential is low or because of a cathodic polarization, the electrode tends to become more active. This can be deduced, for instance, from an increase in the hydrogen evolution. According to Kunze (47) a cathodic Tafel curve is obtained by cathodic polarization. The curve deviates from "normal" Tafel curves on two main points. The Tafel slope is much steeper and both the slope and the position of the curve is time dependent. In general, the electrode polarization decreases with increasing time at low potentials. Some deviations from this picture are, however, observed.

The impurities in the metal play an important role and may determine the reaction rate of the hydrogen evolution. When small amounts of Fe are introduced into Al, the cathodic polarization is seen to decrease, especially at very low potentials (47). At higher potentials the effect is less pronounced.

In the potential range between -1.4 and -1.5 V (SCE) a cathodic limiting current is observed. Fateev *et al* (19) have shown that for 99.995% Al in 1 M KOH the limiting current is due to an increased anodic dissolution which nearly compensates for the increase in the cathodic current due to the hydrogen evolution reaction. In acetate buffered NaCl solutions, Nisancioglu *et al* (57) observed a similar limiting current when 1 S Al (containing 0.26% Fe, 0.09% Si and 0.016% Zn) was used as test electrode. In that case they found, however, that the limiting current probably was due to diffusion of protons to the reaction sites and not to an increase in the anodic current.

Even though the cathodic reaction is dominating at low potentials, the anodic reaction can still be studied separately in this range. By applying a potential step technique, which will be described in Chapter 4, it has been possible to obtain anodic Tafel curves even at low potentials. These are similar to those obtained under anodic polarization (90). The curves are time dependent. They are displaced towards higher current densities when the prepolarization, *i.e.* the polarization before the step, is decreased in cathodic direction.

The anodic reaction can also be detected by analytical methods. Kunze (47) applied such a method in citrate buffered NaCl solutions, and showed that the rate of the Al dissolution reaction reached a minimum at approximately -1.3 V (SCE), whereafter it increased sharply on a further decrease in the potential. Fateev *et al* (19), using a similar method in 1 M KOH solutions, obtained similar results. Going further down in potential than Kunze, they showed that the Al dissolution did not continue to increase with decreasing potential. At approximately -1.8 V (SCE) the dissolution rate reached a maximum. Thereafter, a decrease was observed in a Tafel-like manner. The slope of the new Tafel line seems, however, to be quite steep (~ 0.17 V/log unit).

The resemblance between the results of Kunze and Fateev indicates that the main mechanism of the anodic Al dissolution and the cathodic hydrogen evolution has not changed significantly by going from the weak acid solution (pH = 5) to alkaline solutions. The increased activity observed in both solutions on a decrease in potential is therefore probably connected with changes in the properties of the oxide film covering the metal surface.

1.5 The cathodic break-down potential

Videm (88) has studied the correlation between the oxide film thickness and the formation voltage. The thickness was determined by capacity measurements. The electrode was treated as a parallel plate condenser according to the formula $C = \epsilon_r \epsilon_0 / \delta$, where C is the capacity, ϵ_0 the permittivity in vacuum, ϵ_r the dielectric constant of the oxide, and δ the oxide film thickness.

In tartrate solutions he found excellent agreement between the inverse capacitance and the oxide thickness given by the electrode potential, assuming an anodizing ratio of 14 Å/V. By extrapolating the inverse capacitance to film-free conditions, he found that at an electrode potential of -1.3 V (SHE), *i.e.* -1.55 V (SCE), there should be no film. Comparing this with the results of Kunze and Fateev, it can be seen that -1.55 V (SCE) is in the vicinity of the potential where the anodic current starts to increase. According to Videm, the dissolution of the film is due to the formation of a more stable oxyhydrate (Hydrargirite) which does not influence the capacitance. The formation of this oxide results in a decreased concentration of Al^{3+} ions in the solution. A dissolution of the oxide film will therefore take place due to the higher solubility of the latter.

Formation of a hydrated oxide layer is also suggested by Kunze. Contrary to Videm, however, he does not assume that the oxide film dissolves. He merely assumes that a gradual conversion to a hydrated layer takes place due to proton diffusion into the oxide from the electrolyte. Since the anhydrous oxide film is expected to have electronic conductivity and the hydrous film not, the hydrogen evolution will take place at the anhydrous/hydrous oxide film interface.

Since this interface moves towards the metal phase on a lowering of the electrode potential, both the anodic and the cathodic reactions will be increased. A similar mechanism has also been discussed by Nisancioglu *et al* (57) and DiBari *et al* (13).

The potential at which the film seems to dissolve has been discussed by Nisancioglu *et al* (57). By comparing the results obtained from 1 S Al (*i.e.* relatively impure Al) with values in the literature from super-pure Al, they conclude that the film break-down must be due to alkalization. They indicate that the break-down potential increases linearly with increasing pH. For super-pure Al the slope is 120 mV/pH, while the slope for 1S Al is 60 mV/pH.

As also pointed out by Nisancioglu, some deviations from the pH dependency described above seem to exist. One of the values from Videm (88) does not fit into their plot. A comparison between the data of Fateev obtained using 1 M KOH solutions (19) with those of Kunze at pH=5, shows that the latter seem to be displaced approximately 125 mV in the anodic direction and not in the cathodic direction as expected from the cited pH dependency.

From the discussion above it can be seen that the potential at which no film is present, *i.e.* the cathodic break-down potential, is a disputable but important figure. Several authors have therefore treated the subject (7,38,69,76,93).

In an attempt to determine the potential, Smith (69) made a plot of the inverse capacitance vs the formation voltage, similar to that of Videm. Although mentioned, the double layer capacitance was not taken into account. He therefore extrapolated the results to zero inverse capacitance and obtained a potential of -2.3 ± 0.1 V (SCE), *i.e.* -2.05 ± 0.1 V (SHE). Videm, who did take the double layer capacitance into consideration by assuming that a film-free surface had a similar double layer capacitance to a Pt electrode of equal shape and size, found the potential to be -1.3 V (SHE), as mentioned above. Although the difference in extrapolation may account for some of the deviation in the results, it cannot explain all. Another difference in procedure exists, however, in the two cited works. While the formation voltage still was applied during the measurements of Smith, Videm measured the capacitance without an external DC voltage. Vermilyea (76) used the technique as Smith and Videm on Ta. He found that the capacitance increased with decrease in the voltage during the measurements. He assumed that the decrease was due partly to changes in the double layer capacitance and partly to a change in the dielectric constant of the oxide film. Even though the capacitance is dependent on the voltage, he found the slope of the inverse capacitance vs the formation voltage to remain unchanged. The line was, however, displaced towards higher potential values. Even though these results were obtained for Ta, they are probably valid for Al as well. In that case the remaining difference between the results of Videm and Smith may be explained by a difference in experimental procedure.

As can be seen, many unknown factors seem to be involved in the procedure of extrapolation. The method, therefore, does not provide a reliable means of determining the potential, as also pointed out by Anderson *et al* (7). A value calculated from thermodynamic data seems now to be more generally accepted (7,38). Such calculations show that the break-down potential is pH dependent, and is cathodically displaced on an increase in pH. For Al in solutions of pH = 5.2 it has a value of -2.05 V (SCE). This is in the vicinity, but somewhat higher than the experimentally obtained value of Smith. Similar correlations between calculated and extrapolated values are obtained for several other metals, for instance Ta (93), indicating the general validity of the calculations. A further thermodynamic treatment of the oxide electrode, including the break-down potential, will be given in Chapter 2.

1.6 Film thinning and hydration

If the break-down potential is much lower than the previously expected -1.3 V (SHE), the increase in the cathodic current density must have another explanation.

Vermilyea (76), in his treatment of the oxide film on Ta, has suggested that at low potentials the oxide film becomes gradually thinner. Below a certain potential the film is so thin that electron tunnelling through the oxide from the metal to the solution becomes probable. This will result in an increased transport of electrons through the oxide, whereby the hydrogen evolution will take place at an increased

rate. But, as pointed out by Vermilyea, the field across the oxide will still be anodic in spite of the fact that the total current density may be cathodic.

If the increased hydrogen evolution really is due to film thinning, such thinning must occur when the potential is lowered.

On thick anodic films a thinning, *i.e.* a dissolution of the film, can take place if the potential is lowered. This has clearly been demonstrated by O'Sullivan *et al* (60). After forming a film by anodizing to 115 V, the voltage was reduced to 85 V. The relaxation process was then followed by recording the change in current density and by taking samples for electron microscopic studies at certain intervals. After some time with low current, they observed that the current started to increase until a new and stable value was obtained. The electron microscopic studies showed that a thinning of the barrier layer had taken place immediately after the voltage change. When the current density had reached the stable value, the film thickness had reached a new, stable but thinner value. They claimed that the thinning was due to a "field assisted dissolution". This was demonstrated by comparing the dissolution rate of two oxides. On the first, no field was applied. On the other a decreased, but still high field was present. The film thinning was then observed to be much greater on the oxide with the field than on the oxide without. They therefore concluded that, although some "chemical dissolution" occurred, most of the thinning was due to the "field assisted thinning".

Anderson *et al* (7) have done similar experiments on films formed at 30 V. When the voltage was lowered, they observed a sharp decrease in the current. After a while, the current increased until a new and stable value was reached. The new value was nearly independent of the voltage decrease, even for voltages down to -1.1 V (SCE). They concluded that the increase in current was due to film thinning. When the stable current was reached, the original electric field across the film was reestablished and the film thinning ceased.

Hoar *et al* (38) studied the change in the oxide film during constant voltage of formation. They found that a porous film started to grow, followed by a slight thinning of the barrier layer. The effect was more pronounced at lower pH values. They explained the results by assuming that a "thermal" passage of protons had taken place. The protons moved against the electric field, from the solution into the oxide. The result was a partial hydration of the oxide.

The opposite effect was observed by Schwabe *et al* (68) during an increase in the voltage. Using water containing tritium, they found that the increase in voltage had resulted in a dehydration of the oxide. By using sulphuric acid with S^{35} they found that SO_4^{--} ions were also forced out of the oxide on an increase in voltage. The results were explained as due to electroosmosis.

Rabbo *et al* (62) have studied the film hydration by using secondary ion mass spectrometry. The films were formed in ammonium tartrate solutions of pH = 2.2 to 10.6 with a voltage of formation equal to 60 V. Using the film formed at pH = 6.7 as a standard, they found that a reduced pH resulted in a thinner film. If the pH was increased into the alkaline range, an increase in thickness was observed. Up to a thickness corresponding to that formed at pH = 6.7, the film formed in alkali behaved like those of lower pH. Upon this film a new type of film was formed. The intensity of both AlO^+ and O^+ detected by the mass spectrometer was lower for the new film, indicating that the outer film had a lower density than the inner. They concluded that the outer film probably was porous.

The intensity of H^+ and OH^- was relatively uniformly distributed at all pH values examined, indicating that both the inner and outer films were to some extent hydrated. The degree of hydration was seen to increase with an increase in pH. The result might seem to oppose the earlier assumptions of a barrier layer consisting of an anhydrous oxide. As pointed out by Rabbo, however, the absolute degree of hydration is difficult to estimate from the experiments and may be small.

When the duplex film is formed, it is apparent that the outer film has a higher degree of hydration than the inner. Even if only the barrier film is formed, the outermost part of it seems to be more hydrated than the rest.

1.7 The duplex film

In all the cases where a duplex film was formed, a clearly definable boundary was found between the two film types. The inner part was always nearly identical to the barrier film formed in acid and neutral solutions. As pointed out by Rabbo, "this would suggest strongly that the inner region carries all the field, and the outer region results from attack of a growing inner region". In the most alkaline solution (pH = 10.6) Rabbo *et al* found some deviation from those films formed at lower pH. Although the boundary between the two layers still was sharp, indications were found of a relatively high degree of hydration also of the barrier layer. The barrier layer seems therefore to be attacked by the alkaline solution.

Since the inner region, *i.e.* the barrier layer, carries all the field, the outer region, *i.e.* the porous layer, will have little direct influence on the current density, as also pointed out by Anderson *et al* (7). The electrochemical reactions will therefore mainly take place at the boundary between the barrier and the porous layer. This is also in agreement with the findings of Hoar *et al* (38) who state that the Al dissolution takes place at the pore base. From here the Al^{3+} ions diffuse or migrate through the pores and into the solution. The H^+ ions will move in the opposite direction and be discharged at the barrier layer. A partial hydration of the oxide will therefore have nearly the same effect on the electrochemical reactions as a thinning of the barrier layer.

Even though the porous layer does not have a direct influence on the current density, it may control the transport of ions to and from the barrier layer. This has been described by Nisancioglu *et al* (57). The effect is expected to be very pronounced for cathodic polarization in unbuffered solutions. Here the pH will be much higher in the pores than outside due to the consumption of H^+ ions by the hydrogen evolution reaction. This gives rise to a highly localized attack which is not observed in the buffered solutions (57).

1.8 Other metal oxide films

The formation of a duplex film with an inner barrier layer and an outer hydrated porous layer is not specific for Al. Also an increased hydration of the oxide film by cathodic polarization is found on other metals. Schwabe (68) has shown that dehydration of the oxide takes place when Zn is anodically polarized. The effect is even stronger than that observed for Al since the oxide is thicker.

Laser *et al* (48) have shown that when an anodic oxide film on Ti is cathodically polarized, thinning of the film takes place. But in addition they showed that the optical constants of the film changed. They suggested that the change was due to an injec-

tion of H^+ ions from the solution and electrons from the metal. "Thus H atoms are introduced into the oxide and are probably bound to O^{2-} ions to form OH groups."

A duplex layer with an inner barrier layer and a hydrated porous layer was also found by De Smet (10) on molybdenum. The hydrated layer was formed at the expense of the barrier layer during cathodic polarization. Since the hydrated oxide on Mo is less soluble than the anhydrous barrier layer, it could be shown by simple solubility experiments on partially hydrated films that the hydrated layer was formed from the electrolyte side.

Even on iron a duplex layer is probably formed. Sato *et al* (64) have shown that when Fe is anodized in phosphate or borate solutions, an oxide film consisting of an anhydrous ferric oxide inner layer is formed. While Sato found only Fe^{3+} in the oxide film other authors claim that a partially reduced layer also exists (37,54). In neutral and alkaline solutions Sato found that an outer hydrous ferric oxide is formed. In acid solutions only the barrier layer is formed, precisely as for Al. The main part of the electric field on iron is also assumed to appear across the barrier layer. No appreciable potential drop is expected in the deposit layer, *i.e.* the porous film. As for other anodic duplex films, the hydrated layer seems to be affected significantly by changes in the solution, such as changes in pH and anions. The barrier layer, on the other hand, depends on the potential but hardly on the environment. In acid solutions, however, a thinning is observed similar to that observed for Al.

1.9 The Al electrode in aqueous solution

From the foregoing it can be seen that the electrochemical behaviour of Al in aqueous solutions is closely related to the properties of the oxide film. The active Al electrode is nearly impossible to study in aqueous solutions due to the un noble character of Al and the ease with which it forms an oxide film. Even in strongly alkaline solutions where the oxide film is unstable, the dissolution of Al still takes place via an anodic film, as also pointed out by Heusler *et al* (34).

The study of Al in aqueous solutions will therefore inevitably be a study of a passive metal.

Although the oxide film on Al at first glance seems to be unique, many parallels to other passive metals seem to exist. The similarities are most strikingly seen for metals like Ti, Nb and Ta, but as pointed out above, a comparison to iron and molybdenum may also prove valuable. This should be borne in mind when studying the electrochemistry of Al in aqueous solutions.

2 THERMODYNAMIC CONSIDERATIONS

2.1 General

Vetter (83,84,85) has in a series of articles treated oxide-covered metal electrodes from a thermodynamic point of view. The results of these considerations have been used to interpret results from experiments on passive metals like iron (86,92), nickel (92) and titanium (2). The treatment is of a general nature, however, and not limited to the use on these metals. It is therefore worthwhile to look further into the subject, with the passivity of Al in mind.

The general scheme used by Vetter is shown in Figure 2.1. It is a cell composed of an oxide-covered metal electrode combined with a reversible hydrogen electrode in contact with a common electrolyte.

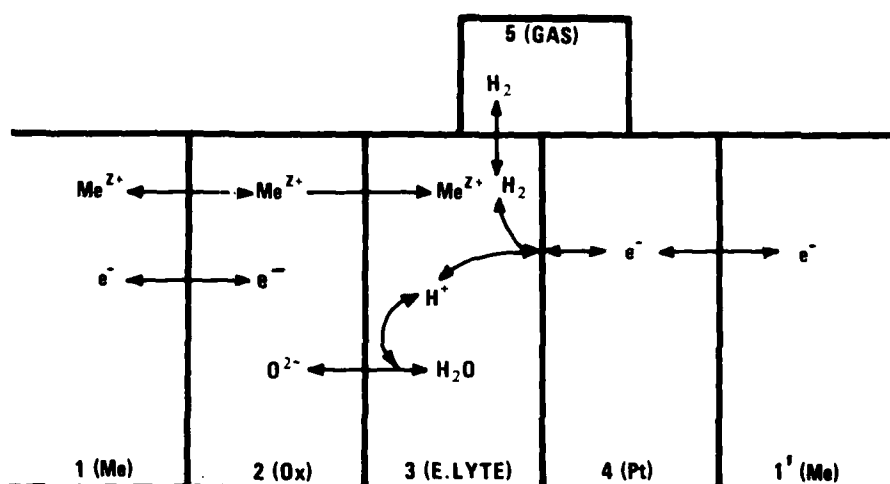


Figure 2.1 Schematic diagram of an oxide covered metal electrode connected to a hydrogen electrode (85)

At each interface, charge transfer reactions may take place. If one of these reactions is reversible at an interface, the potential difference (pd) at this interface must be equal to the reversible potential of the reaction. As such, it is determined by the thermodynamic conditions at the interface. The other reactions taking place at the same interface will have no direct influence on the pd. They will act only through their eventual influence on the thermodynamic conditions.

In Figure 2.1 neither the hydrogen evolution at the oxide electrode nor the oxygen reduction is taken into account. When they occur at the oxide-electrolyte interface, a transport of electrons through the oxide takes place. H^+ ions may, however, diffuse through the oxide. In that case the H^+ ions may exchange electrons directly with the metal.

Even though both hydrogen evolution and oxygen reduction may proceed in parallel with the reactions in the figure, a very complicated picture will arise if all the

reactions are taken into account at once. For reasons of clarity the hydrogen evolution and the oxygen reduction are omitted here. Later on, the hydrogen evolution reaction will be taken into consideration.

2.2 The metal-oxide interface

As shown in Figure 2.1, two exchange reactions take place at the metal-oxide interface. For Al these reactions are



One of them, or both, may be at equilibrium. If both, only a certain composition of the oxide can exist in contact with the metal. This oxide must fulfil the thermodynamic conditions given by the two equilibrium reactions, but need not be a stoichiometric oxide. The μ at the interface will then have a fixed value. Vetter called this oxide "the equilibrium oxide". He points out that for oxide covered iron the equilibrium oxide has a composition in the vicinity of Fe_3O_4 (84).

Wagner (92) has given the oxide on iron a further treatment. He points out that Fe_3O_4 is a mixed oxide containing both Fe^{3+} and Fe^{2+} ions. It has an inverse spinel structure and 1/3 of the Fe ions are in the divalent state, the remaining 2/3 are in the trivalent state. Half of the Fe^{3+} ions and all the Fe^{2+} ions occupy the octahedral sites. The remaining Fe^{3+} ions occupy the tetrahedral sites.

When the oxide is oxidized, some of the Fe^{2+} ions are converted to Fe^{3+} ions. For electroneutrality reasons, some Fe ions are at the same time forced out of the lattice. In the end, the oxide will contain mostly Fe^{3+} ions and have a composition $\text{Fe}_{2.67}\text{O}_4$ with 1/9th of the normal cation sites vacant. This oxide is identical to $\gamma\text{-Fe}_2\text{O}_3$ and has still the inverse spinel structure.

Verwey (79,80) has shown that the oxide formed on anodized Al is $\gamma'\text{-Al}_2\text{O}_3$. The oxide has an inverse spinel structure, too. 70% of the Al^{3+} ions are on octahedral sites and the remaining 30% are on tetrahedral sites. The Al^{3+} ions are statistically distributed on these sites. The situation is therefore very similar to that observed for iron. But contrary to iron, ions of lower valency than three are very rare. An oxide corresponding to Fe_3O_4 is therefore hardly to be expected. Hartmann (29) has shown, however, that when $\alpha\text{-Al}_2\text{O}_3$ is heated in vacuum (450°C and 10^{-4} mm Hg), the electronic conductivity is increased from below $10^{-9} \Omega^{-1}\text{m}^{-1}$ to $10^{-5} \Omega^{-1}\text{m}^{-1}$. When oxygen was added, the conductivity decreased while an increase in conductivity was observed when hydrogen was added. The effect was explained by assuming that a partial reduction takes place when the oxide is heated in vacuum or in hydrogen. The reduction results in an oxide with metal excess similar to that observed on iron. After the reduction was completed, the temperature was lowered and the change in conductivity was measured. A decrease in conductivity with a decrease in temperature was found. The decrease corresponded to that expected when no change in the oxide had taken place during the cooling. It was therefore obvious that the reduced state was still present at room temperature. This demonstrates that partially reduced oxides may exist also at room temperature. "The equilibrium oxide" on Al is probably such a partially reduced oxide, although not in the same degree of reduction as on iron. It is also likely that the reduced oxide has a relatively good electronic conductivity.

When an anodic steady-state current is flowing, Al^{3+} ions will migrate through the oxide from the metal to the solution. The equilibrium between Al^{3+} ions in the metal and in the oxide may then disappear. The electronic equilibrium may, however, still

be maintained. If a considerable amount of H_2 is evolved, as may be the case when a high cathodic current is flowing, the condition of electronic equilibrium may not be fulfilled. The electrons are then consumed according to the reaction



which may be so fast that electronic equilibrium cannot be established. The assumption of electronic equilibrium may, however, be valid if the electronic conductivity is good. In that case the electrochemical potential of the electrons in the metal equals that in the oxide, and we have

$$\mu_e(me) - F\varphi(me) = \mu_e(ox) + F\varphi(ox) \quad (2.4)$$

where $\mu_e(me)$ – chemical potential of the electrons in the metals
 $\mu_e(ox)$ – chemical potential of the electrons in the oxide
 $\varphi(me)$ – potential of the metal
 $\varphi(ox)$ – potential of the oxide
 F – Faraday constant

Since $\mu_e(me)$ and $\varphi(me)$ are considered constant, we then have

$$d\mu_e(ox) = Fd\varphi(ox) \quad (2.4')$$

which shows that the chemical potential of the electrons changes linearly with an increase in the pd at the metal-oxide interface.

As pointed out by Wagner (92) for iron, the cation in the oxide may formally be treated as a dissociation product of metal dissociation. For Al this formal dissociation may be written



resulting in the thermodynamic equation

$$d\mu_{Al}(ox) = d\mu_{Al^{3+}}(ox) + 3d\mu_{e^-}(ox) \quad (2.6)$$

where $\mu_{Al}(ox)$ – chemical potential of Al in the oxide
 $\mu_{Al^{3+}}(ox)$ – chemical potential of Al^{3+} ions in the oxide

Combined with Equation (2.4') it gives

$$d\mu_{Al}(ox) = \frac{d\mu_{Al^{3+}}(ox)}{d\mu_{Al}(ox)} d\mu_{Al}(ox) + 3Fd\varphi(ox) \quad (2.7)$$

If $\mu_{Al}(ox)_0$, $\mu_{Al^{3+}}(ox)_0$ and $\varphi(ox)_0$ are the thermodynamic parameters of the equilibrium oxide, an integration of Equation (2.7) gives

$$\mu_{Al}(ox) - \mu_{Al}(ox)_0 = \int_{\mu_{Al}(ox)_0}^{\mu_{Al}(ox)} \frac{d\mu_{Al^{3+}}(ox)}{d\mu_{Al}(ox)} d\mu_{Al}(ox) + 3F(\varphi(ox) - \varphi(ox)_0) \quad (2.8)$$

The equation is similar to that given by Wagner for iron, and shows the deviation of $\mu_{\text{Al}}(\text{ox})$ from its equilibrium value as a function of the potential and the Al^{3+} variation in the oxide at the metal-oxide interface.

Since the oxide has a composition in the vicinity of $\gamma\text{Al}_2\text{O}_3$, large amounts of cation vacancies exist. The chemical potential of the electrons will therefore, according to Wagner, vary steeply with a change in $\mu_{\text{Al}}(\text{ox})$ while $\mu_{\text{Al}^{3+}}(\text{ox})$ will be virtually independent of such a change. In that case the integral in Equation (2.8) will tend towards a limiting value, *i.e.*

$$\int_{\mu_{\text{Al}}(\text{ox})_0}^{\mu_{\text{Al}}(\text{ox})} \frac{d\mu_{\text{Al}^{3+}}(\text{ox})}{d\mu_{\text{Al}}(\text{ox})} d\mu_{\text{Al}}(\text{ox}) \rightarrow 1 \quad (2.9)$$

$$\mu_{\text{Al}}(\text{ox}) \rightarrow -\infty$$

Since even the equilibrium oxide probably has a composition which does not deviate significantly from $\gamma\text{Al}_2\text{O}_3$, the integral is virtually constantly equal to 1. In that case Equation (2.8) becomes equal to

$$\mu_{\text{Al}}(\text{ox}) - \mu_{\text{Al}}(\text{ox})_0 = 1 + 3F(\varphi(\text{ox}) - \varphi(\text{ox})_0) \quad (2.10)$$

which shows that not only the chemical potential of the electrons but also the chemical potential of Al will change linearly with a change in the potential of the metal-oxide interface.

When the potential of the oxide is lowered relative to the metal, *i.e.* the electrode is anodically polarized, the concentration of the electrons and Al in the oxide is expected to decrease exponentially since an approximately logarithmic connection exists between the chemical potential and the concentration. The oxide becomes more insulating. On the other hand, the oxide should be more conducting when the potential is increased, *i.e.* the electrode is cathodically polarized.

Heusler (33) has treated the reactions at the metal-oxide interface. By extrapolating the rate of oxygen dissolution in metals from elevated temperatures to room temperature, he reached the value $10^{-15} \text{ A cm}^{-2}$ for this reaction rate. Assuming this to be the upper limit of the metal exchange reaction at the interface, he concludes that substantial overvoltage for the metal transfer across the oxide metal interface must exist during anodic oxidation of metals. In that case the oxide in contact with the metal may be far from the equilibrium oxide. As shown above it may, however, still have a composition in the vicinity of $\gamma\text{Al}_2\text{O}_3$.

2.3 The oxide-electrolyte interface

According to Figure 2.1 the two reactions that take place at the oxide-electrolyte interface comprise the oxygen exchange reaction



and the Al dissolution reaction



While Reaction (2.11) can proceed in both directions and may also be an equilibrium reaction, Reaction (2.12) can usually only proceed in one direction, *i.e.* in the direction from the oxide to the solution (83).

Since only a negligible amount of oxygen usually dissolves in the metal, the oxide has to increase in thickness if Reaction (2.11) shall proceed from left to right. Reaction (2.11) is therefore inevitably connected to the formation of the oxide. When the oxide growth ceases, Reaction (2.11) will reach equilibrium, and when the oxide thickness decreases, it will proceed from right to left.

In steady state, there is no change in thickness. Reaction (2.11) will then be an equilibrium reaction and the thermodynamic conditions must be obeyed. The pd between the oxide and the electrolyte is then given by the equation

$$\varphi(\text{ox}) - \varphi(\text{el}) = \frac{1}{2}F [\mu_{\text{O}^{2-}}(\text{ox}) + 2\mu_{\text{H}^+}(\text{el}) - \mu_{\text{H}_2\text{O}}(\text{el})] \quad (2.13)$$

$\mu_{\text{O}^{2-}}(\text{ox})$ – chemical potential of the oxygen ions in the oxide

$\mu_{\text{H}^+}(\text{el})$ – chemical potential of the hydrogen ions in the electrolyte

$\mu_{\text{H}_2\text{O}}(\text{el})$ – chemical potential of water in the electrolyte, virtually equal to $\Delta G_f^\circ(\text{H}_2\text{O})$

The equation shows that the pd depends only on the oxide composition ($\mu_{\text{O}^{2-}}(\text{ox})$) and on the pH of the electrolyte ($\mu_{\text{H}^+}(\text{el})$). Since the oxide is virtually $\gamma\text{-Al}_2\text{O}_3$, $\mu_{\text{O}^{2-}}(\text{ox})$ is not expected to deviate significantly from that in pure $\gamma\text{-Al}_2\text{O}_3$. $\mu_{\text{O}^{2-}}(\text{ox})$ is therefore assumed to be constant. In that case the pd between the oxide and the electrolyte depends in steady state only on the pH.

The reaction rate of Al dissolution at the oxide–electrolyte interface *i.e.* Reaction (2.12) is a function of the surface concentration of Al^{3+} ions at the oxide surface and the pd across the interface. This pd is the same as that for the oxygen ion exchange reaction. In steady state it will therefore depend only on the pH of the solution. Since the oxide composition is not expected to change significantly, the surface Al^{3+} ion concentration is also expected to be nearly constant. In that case the Al dissolution reaction should be independent of the total electrode potential and only dependent on the pH of the solution.

If pH is introduced into Equation (2.13), the following equation is derived

$$\varphi(\text{ox}) - \varphi(\text{el}) = \frac{1}{2}F [\mu_{\text{O}^{2-}}(\text{ox}) + 2\mu_{\text{H}^+}^0(\text{el}) - \mu_{\text{H}_2\text{O}}(\text{el})] - 2.303 \frac{RT}{F} \text{pH} \quad (2.14)$$

where $\mu_{\text{H}^+}^0(\text{el})$ chemical potential of the hydrogen ions in standard state *i.e.* zero

The equation shows that the pd at the interface will decrease 60 mV per unit increase in pH.

When Allard *et al* studied the reactions on oxide covered Ti electrodes, the Ti dissolution reaction was also treated (2). An equation similar to their dissolution equation for Ti can also be used for the Al dissolution reaction on the oxide covered Al-electrode, *i.e.*

$$j_c = k_c^+ a_{\text{Al}^{3+}}^2 \cdot a_{\text{H}^+}^3 \exp [\gamma (F E_{23} / RT)] \quad (2.15)$$

where	j_c	- Al dissolution rate
	k_c^*	- rate constant
	$2a_{Al^{3+}}$	- activity of Al^{3+} in the oxide surface
	$3a_{H^+}$	- activity of H^+ ions in the electrolyte
	$E_{2,3}$	pd between the oxide and the electrolyte
	z	- reaction order of H^+
	γ	- effective transfer coefficient of the Al dissolution

Combining this equation with Equation (2.14) gives the pH dependency of the Al dissolution reaction

$$\log j_c = \log(k_c^* 2a_{Al^{3+}}) + \frac{\gamma}{2.303 \cdot 2RT} \mu + (z-\gamma)pH \quad (2.16)$$

μ is the sum of chemical potentials in the bracket in Equation (2.14).

The equation shows that the logarithm of the Al dissolution rate is linearly dependent on pH with a slope equal to $z-\gamma$.

Kaesche (43) has in fact observed a stationary potential independent anodic dissolution current which he called an anodic limiting current. In the pH range 7 to 11.5 he found a linear correlation between the logarithm of the current and the pH, just as expected from the above discussion. The slope of the line corresponding to $z-\gamma$ was somewhat below 1 (~ 0.95). It was not dependent on whether chloride or sulphate ions were used in the electrolyte. The chloride line had, however, a small displacement towards higher current densities when compared with the SO_4^{2-} line. The limiting current increased, however, when the electrolyte was buffered and decreased with increasing stirring. The slope of the lines can therefore not directly be used to determine $z-\gamma$ since diffusion in the electrolyte obviously plays a certain role.

Potential independent steady-state anodic current has also been observed on iron (82), chromium (8) and cobalt (65). The potential independent current is also on these metals pH dependent. The slope is negative, however, giving a negative value of $z-\gamma$. For Fe, at least, this is also to be expected since $z=0$ (4). The same may perhaps be the case for Cr and Co.

The "potential independent" dissolution rate of Al and its pH dependency will be treated in Chapter 3.

2.4 The oxide film

The oxide film has two boundary phases, *i.e.* the metal-oxide interface and the oxide-electrolyte interface. The reactions taking place at these interfaces will determine the potential of the oxide. The oxide may not, however, have the same potential at the two interfaces. If the potentials are different, an electric field will be established across the oxide film.

Instead of one potential for the oxide, *i.e.* $\varphi(ox)$, it might be valuable to operate with two, one for the potential at the metal-oxide interface, $\varphi'(ox)$, and one for the potential at the oxide-electrolyte interface, $\varphi''(ox)$. The pd across the oxide will then be $\varphi''(ox) - \varphi'(ox)$. Wagner (92) has expressed this difference by Equation (2.8), but

this time integrating between the conditions at the two interfaces, i.e.

$$\varphi''(\text{ox}) - \varphi'(\text{ox}) = \frac{1}{3F} (\mu''_{\text{Al}}(\text{ox}) - \mu'_{\text{Al}}(\text{ox})) - \frac{1}{3} \int_{\mu'_{\text{Al}}(\text{ox})}^{\mu''_{\text{Al}}(\text{ox})} \frac{d\mu_{\text{Al}^{3+}(\text{ox})}}{d\mu_{\text{Al}}(\text{ox})} d\mu_{\text{Al}}(\text{ox}) \quad (2.17)$$

where $\mu'_{\text{Al}}(\text{ox})$ — chemical potential of Al in the oxide towards the metal
 $\mu''_{\text{Al}}(\text{ox})$ — chemical potential of Al in the oxide towards the electrolyte

According to Equation (2.9), the integral will approach a constant limit I when $\mu_{\text{Al}}(\text{ox}) \rightarrow -\infty$, i.e. under anodic conditions. Equation (2.17) can then be written

$$\varphi''(\text{ox}) - \varphi'(\text{ox}) \rightarrow \frac{1}{3F} (\mu''_{\text{Al}}(\text{ox}) - \mu'_{\text{Al}}(\text{ox})) - \frac{1}{3} I \quad (2.18)$$

when $\mu_{\text{Al}}(\text{ox}) \rightarrow -\infty$

showing that the pd across the oxide is linearly dependent on the difference in chemical potential of Al, i.e. $\mu_{\text{Al}}(\text{ox})$, at the two interfaces.

The electrode potential, i.e. the total pd between the metal and the electrolyte relative to a reference electrode, can be divided into the following pd's

$$E = \varphi(\text{me}) - \varphi(\text{el}) + \Delta\varphi_r = (\varphi(\text{me}) - \varphi'(\text{ox})) + (\varphi'(\text{ox}) - \varphi''(\text{ox})) + (\varphi''(\text{ox}) - \varphi(\text{el})) + \Delta\varphi_r \quad (2.19)$$

$\Delta\varphi_r$ is the pd of the reference electrode.

The pd across the oxide is given by the equation

$$\varphi''(\text{ox}) - \varphi'(\text{ox}) = (\varphi(\text{me}) - \varphi'(\text{ox})) + (\varphi''(\text{ox}) - \varphi(\text{el})) + \Delta\varphi_r - E \quad (2.20)$$

When electronic equilibrium is assumed across the metal-oxide interface, the pd across this interface is given by Equation (2.4), i.e.

$$\varphi(\text{me}) - \varphi'(\text{ox}) = \frac{1}{F} [\mu_e(\text{me}) - \mu'_e(\text{ox})] \quad (2.4)$$

where $\mu_e(\text{me})$ — chemical potential of the electrons in the metal
 $\mu'_e(\text{ox})$ — chemical potential of the electrons in the oxide towards the metal

The pd of the oxide-electrolyte interface under steady state conditions is given by Equation (2.14), i.e.

$$\varphi''(\text{ox}) - \varphi(\text{el}) = \frac{1}{2F} [\mu''_{\text{O}^{2-}}(\text{ox}) + 2\mu_{\text{H}^+}^0(\text{el}) - \mu_{\text{H}_2\text{O}}(\text{el})] - 2.303 \frac{RT}{F} \text{pH} \quad (2.14)$$

where $\mu''_{\text{O}^{2-}}(\text{ox})$ — chemical potential of the oxygen ions in the oxide towards the electrolyte

When Equations (2.4) and (2.14) are introduced into Equation (2.20), the equation becomes

$$\begin{aligned} \varphi''(\text{ox}) - \varphi'(\text{ox}) = & \frac{1}{F} [\mu_e^-(\text{me}) - \mu_e^-(\text{ox})] + \frac{1}{2F} [\mu_{\text{O}^{2-}}''(\text{ox}) + 2\mu_{\text{H}^+}^0(\text{el}) - \mu_{\text{H}_2\text{O}}(\text{el})] \\ & - 2.303 \frac{RT}{F} \text{pH} + \Delta\varphi_r - E \end{aligned} \quad (2.21)$$

Using the formal equilibrium



the chemical potential of the electrons in the oxide is given by the equation

$$\mu_e^-(\text{ox}) = \frac{1}{3} \mu_{\text{Al}}(\text{ox}) - \frac{1}{3} \mu_{\text{Al}^{3+}}(\text{ox}) \quad (2.22)$$

When the oxide has a stoichiometry in the vicinity of $\gamma\text{-Al}_2\text{O}_3$, we also have the formal equilibrium



which states that

$$\Delta G_{\text{Al}_2\text{O}_3} = 2\mu_{\text{Al}^{3+}}(\text{ox}) + 3\mu_{\text{O}^{2-}}(\text{ox}) \quad (2.24)$$

When the Equations (2.22) and (2.24) are introduced into Equation (2.21), the following equation is derived

$$\begin{aligned} \varphi''(\text{ox}) - \varphi'(\text{ox}) = & \frac{1}{F} [\mu_e^-(\text{me}) - \mu_{\text{H}^+}^0(\text{el}) - \frac{1}{2} \mu_{\text{H}_2\text{O}}(\text{el}) + \frac{1}{6} \Delta G_{\text{Al}_2\text{O}_3}^0] \\ & - \frac{1}{F} \mu_{\text{Al}}(\text{ox}) - 2.303 \frac{RT}{F} \text{pH} + \Delta\varphi_r - E \end{aligned} \quad (2.25)$$

Where

$$\mu_{\text{Al}^{3+}}'(\text{ox}) \approx \mu_{\text{Al}^{3+}}(\text{ox})$$

$$\mu_{\text{O}^{2-}}''(\text{ox}) \approx \mu_{\text{O}^{2-}}(\text{ox})$$

The expression in the first bracket on the right hand side of Equation (2.25) will have a constant value $K(\text{ox})$, which can be calculated from thermodynamic data. According to JANAF (40)

$$\Delta G_{\gamma\text{-Al}_2\text{O}_3}^0 = -373.790 \text{ kcal/mol}$$

$$\Delta G_{\text{H}_2\text{O}}^0 \approx \mu_{\text{H}_2\text{O}} = -56.690 \text{ kcal/mol}$$

The constant $K(\text{ox})$ divided by Faraday's constant will then have the value

$$\frac{1}{F} K(\text{ox}) = -1.472 \text{ V(SHE)}$$

Since this value is referred to standard hydrogen electrode (SHE), $\Delta\varphi_r$ is included in the constant and Equation (2.25) becomes

$$\varphi''(\text{ox}) - \varphi'(\text{ox}) = -1.472 \text{ V(SHE)} - \frac{1}{F} \mu'_{\text{Al}}(\text{ox}) - 2.303 \frac{RT}{F} \text{pH} - E \quad (2.25')$$

which shows the connection between the pd across the oxide and the electrode potential when the electrode is at steady state. As can be seen, both the pH of the solution and the chemical potential of Al in the oxide are involved.

Experimental data on Al (69,88) and on other passive metals (64,76,93) all indicate that in the anodization region a linear correlation exists between the electrode potential and the oxide film thickness at steady state. The electrode potential can therefore in that region be written as

$$E = E(0) + \delta/U \quad (2.26)$$

where $E(0)$ — electrode potential extrapolated to zero film thickness
 U — anodization ratio
 δ — oxide film thickness

If this is introduced into Equation (2.25') and combined with Equation (2.18), which is also valid in the anodization region, the following equation is obtained

$$E = E(0) + \delta/U = -1.472 \text{ V(SHE)} - 2.303 \frac{RT}{F} \text{pH} - \frac{1}{3F} (\mu''_{\text{Al}}(\text{ox}) - \mu'_{\text{Al}}(\text{ox})) - \frac{1}{F} \mu'_{\text{Al}}(\text{ox}) + \frac{1}{3F} I \quad (2.27)$$

Since $\mu''_{\text{Al}}(\text{ox}) \rightarrow \mu'_{\text{Al}}(\text{ox})$ when $\delta \rightarrow 0$, an extrapolation of E vs δ to zero thickness, i.e. $\delta = 0$, should give

$$E(0) = -1.472 \text{ V(SHE)} - 2.303 \frac{RT}{F} \text{pH} - \frac{1}{F} \mu'_{\text{Al}}(\text{ox}) + \frac{1}{3F} I \quad (2.28)$$

The experimentally observed values of $E(0)$ for Al are not far from the value $(-1.472 \text{ V (NHS)} - 2.303 \text{ RT/F pH})$ (69). Also for other metals the extrapolated $E(0)$ corresponds well with the thermodynamic value obtained when ignoring the terms $\mu'_{\text{Al}}(\text{ox})$ and I (64,76,93). This gives a strong indication that the absolute values of both $\mu'_{\text{Al}}(\text{ox})$ and I are small. This again indicates that $\mu'_{\text{Al}}(\text{ox})$ will not deviate much from that expected if metallic equilibrium had been established between the metal and the oxide. In that case $\mu'_{\text{Al}}(\text{ox}) = \mu_{\text{Al}}(\text{me}) = 0$ by definition. Such an equilibrium has also been assumed by for instance Wagner (92) in treating the passivity of iron. Unfortunately, the extrapolated data obtained from experiments are not good enough to give an acceptable indication of the real values of $\mu'_{\text{Al}}(\text{ox})$ and I .

If the assumptions made above are correct, Equation (2.27) should be valid, not only in the anodization region, but even at low electrode potentials. The connection between the electrode potential at steady state, E_{stab} , and the oxide thickness should then be given by the equation

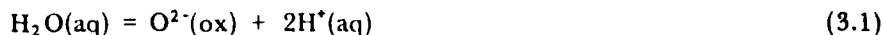
$$E_{\text{stab}} = E(0) + \delta/U$$

where $E(0)$ — $-1.472 \text{ V (NHS)} - 2.303 \text{ RT/F pH}$
 U — anodization ratio
 δ — oxide film thickness

3 REACTIONS AT THE OXIDE-ELECTROLYTE INTERFACE

3.1 General

As pointed out in the previous chapters, the main reactions which are taking place at the oxide-electrolyte interface are the oxide formation and the metal ion dissolution reactions. If the oxide has sufficient electronic conductivity or if it is thin enough for electron tunnelling, red-ox reactions like the hydrogen and oxygen evolution reactions may also take place. Even though all these reactions can be treated independently, they depend on the same pd, i.e. the pd across the oxide-electrolyte interface. The oxide formation can be described as a transfer of oxygen ions from the electrolyte to the oxide with the overall rate equation (83,84,85)



If the reaction proceeds from left to right, an increase in layer thickness is observed. A decrease occurs when the reaction proceeds in the opposite direction. When steady state is reached, Reaction (3.1) can be treated as an equilibrium reaction, and the pd across the oxide-electrolyte interface becomes equal to the equilibrium potential of Reaction (3.1).

The metal dissolution reaction can simply be represented by the following overall equation



In most cases of passivity, this reaction is not an equilibrium reaction, but proceeds nearly always from left to right (83).

Even though Reactions (3.1) and (3.2) both depend on the same pd, the potential may be an equilibrium potential for Reaction (3.1) and not for Reaction (3.2).

A major problem in the study of the reactions at the interface is that the pd across this interface is not known. Only the total pd between the metal and the electrolyte can be measured. Since the pd across the interface is only a part of the total pd, a complicated picture will arise when the reactions are related to the total pd. Other methods, not involving the pd, may therefore preferentially be used when the reactions are studied.

Using an analytical method, Vetter *et al* (86) and Heusler (31) studied the reactions at the oxide-electrolyte interface of passive iron in acid sulphate solutions. A similar method was also used by Allard *et al* on titanium (2). They all found that Reaction (3.1) proceeds in several steps, the first step being



This step could be treated as an equilibrium reaction both for oxide covered Ti and Fe. On Fe, Vetter found the second and rate determining step to be



With a true charge transfer coefficient $\alpha_1 = 0.43$.

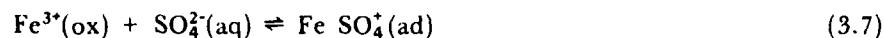
For Ti, Allard *et al* found it necessary to divide the last reaction into two steps





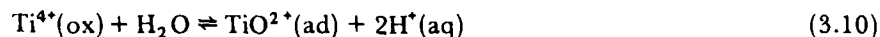
the chemical reaction (3.6) being rate determining.

The iron dissolution corresponding to Reaction (3.2) was found to be independent of pH but dependent on the sulphate concentration. The reaction proceeds in three steps:

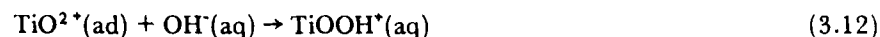


Here Reaction (3.7) is treated as an equilibrium reaction. The rate determining charge transfer, Reaction (3.8), has a charge transfer coefficient $\alpha = 0.52$.

While Vetter found the iron dissolution to be pH independent, a pH dependency of titanium dissolution was found by Allard *et al.* In acid solutions they divided Reaction (3.2) into the following steps



In alkaline solutions the reaction corresponding to Equation (3.11) becomes



The rate determining charge transfer reactions (3.11) and (3.12) have both a charge transfer coefficient $\alpha = 0.27$.

The surface reactions on anodized aluminium have been studied by Gorn (25) using ellipsometry. Based on the changes in the oxide film thickness he found that in acid and neutral sulphate solutions Reaction (3.1) could be divided into the following steps



In accordance with the results on Fe and Ti he found that the first step could be treated as an equilibrium reaction. He states that Reaction (3.13) is rate determining.

For the Al-dissolution reaction he found the following rate determining reaction



One problem in using thickness measurements as a means of determining the partial current densities is that the current efficiency for the oxide formation is usually large, and in neutral solutions it becomes nearly 100%. Since the rate of metal dissolution is determined as the difference between the total current density and the current density of the oxide formation, some uncertainty must be present.

When studying the reactions on Ti, Allard *et al* determined the dissolution rate explicitly by analysing the dissolved Ti ions. The same technique has also been used on

oxide covered Al (91). These experiments will be treated further since they describe the reactions at the oxide-electrolyte interface on oxide covered Al quite well.

3.2 "Tafel" curves of the reactions

Since the pd across the oxide-electrolyte interface cannot be measured directly, Tafel curves of the reactions cannot be determined directly, either. Indirectly, however, the Tafel curves can be found by studying the rates of the different reactions which take place at the interface and which therefore depend on the same pd.

The rate-potential dependency of the oxide formation reaction, *i.e.* Reaction (3.1), is given by the general equation

$$j_{\text{ox}} = k_{\text{ox}}^+ 3a_{\text{H}^+}^y \exp[\beta FE_{2,3}/RT] - k_{\text{ox}}^- 2a_{\text{O}^{2-}} \cdot 3a_{\text{H}^+}^{(2-y)} \exp[-(2-\beta)(FE_{2,3}/RT)] \quad (3.15)$$

where $k_{\text{ox}}^+, k_{\text{ox}}^-$ — Rate constants
 $3a_{\text{H}^+}$ — Activity of H^+ in the electrolyte
 $2a_{\text{O}^{2-}}$ — Activity of O^{2-} in the oxide
 β — Effective transfer coefficient for the oxide formation
 y — The reaction order with respect to H^+
 E_{23} — The pd across the oxide-electrolyte interface
 F, R, T — Have their usual meaning

When an anodic current flows, *i.e.* the oxide grows, the last term in Equation (3.15) can usually be neglected. The rate of oxide growth is then given by the equation

$$j_{\text{ox}} = k_{\text{ox}}^+ 3a_{\text{H}^+}^y \exp[\beta FE_{2,3}/RT] \quad (3.16)$$

This rate can be determined experimentally either by thickness measurements (ellipsometry (25)), by potential measurements or by the difference between the total current density and the partial current density of the metal dissolution reaction (2,91).

The rate of metal dissolution can be described by a similar equation

$$j_{\text{c}} = k_{\text{c}}^+ 2a_{\text{Al}^{3+}} \cdot 3a_{\text{H}^+}^z \exp[\gamma FE_{2,3}/RT] \quad (3.17)$$

where k_{c}^+ — Rate constant
 $2a_{\text{Al}^{3+}}$ — Activity of Al^{3+} in the oxide
 γ — Effective transfer coefficient for the Al-dissolution reaction
 z — Reaction order with respect to H^+

The rate of this reaction can be determined either by the difference between the total current density and the partial current density of the oxide formation determined by ellipsometry (25) or by analytical methods (91).

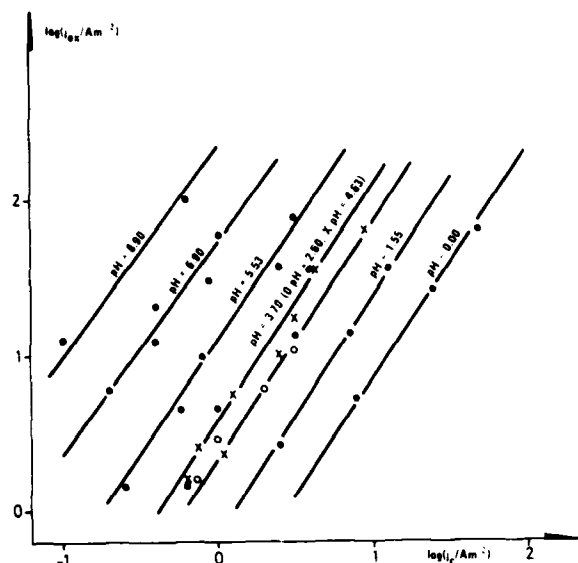


Figure 3.1 The rate of oxide formation as a function of the Al dissolution rate in acid and neutral pH-range

3.3 The pH dependency of the reactions

Equations (3.16) and (3.17) show that if z and y are zero, the reactions are pH independent. Figure 3.1 shows, however, that even though the slopes of the lines are pH independent, the position of the lines is highly dependent on it, indicating that either y , z or both are different from zero.

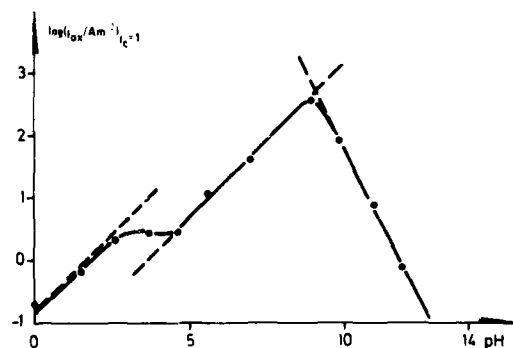


Figure 3.2 The rate of oxide formation at a certain Al dissolution rate (1 A m^{-2}) as a function of pH

The data obtained from the different slopes in Figure 3.2 and the constant slope of the lines in Figure 3.1 give good indications that the rate of oxide formation follows the equation

$$j_{\text{ox}} = k_{\text{ox}} 3 a_{\text{H}^+}^2 \exp \left(\frac{2F}{RT} E_{2,3} \right) \quad (3.18)$$

By combining the Equations (3.16) and (3.17), $E_{2,3}$ can be eliminated. If both involved reactions proceed independently and both follow Tafel's law, the resulting equation shows that a straight line should be obtained if $\log j_{\text{ox}}$ is plotted vs $\log j_c$ for different total current densities. The slope of the line will then be the ratio between the two transfer coefficients, i.e. β/γ .

In Figure 3.1 such a plot is shown for oxide covered Al in acetic acid buffered solutions of different pH values (91). As can be seen, straight lines are in fact obtained. The figure shows that $\beta/\gamma \approx 1.5$ and is independent of pH.

The combination of Equations (3.16) and (3.17) shows that if y and z are unchanged, a straight line should be obtained when $\log j_{\text{ox}}$ at a constant j_c is plotted vs pH. The slope of the line should be equal to $y - z\beta/\gamma$.

In Figure 3.2 such a plot is shown. As can be seen, several lines with different slopes are obtained. Since β/γ is constant, the change in slope indicates that at least one of the reactions has changed reaction order with respect to H^+ when going from neutral to alkaline solutions.

which indicates a reaction mechanism with the following steps



with Reaction (3.21), *i.e.* the incorporation of O^{2-} ions into the oxide, as the rate determining step (91). Since the concentration of $\text{O}^{2-}(\text{ad})$ is dependent on the preceding steps, *i.e.* Reactions (3.19) and (3.20), the reaction rate is highly potential dependent.

The rate of the cathodic oxide dissolution is probably determined by the formation of $\text{O}^{2-}(\text{ad})$ from lattice O^{2-} , *i.e.* Reaction (3.21) in opposite direction. The potential will here act only on the short distance from the oxide to the adsorbed state. It is therefore reasonable to believe that the potential dependency of the dissolution process is much weaker than in the oxide formation process. This may explain why the thickness of the oxide can be increased very fast by an increase in the potential while a thinning can take time, even when the potential is lowered substantially.

While the oxide formation has a constant reaction order with respect to H^+ ions, the metal dissolution reaction has two different reaction orders, one below $\text{pH} = 9$ and one above.

Below $\text{pH} = 9$ is the rate of metal dissolution given by the equation

$$j_c = k_c {}_3a_{\text{H}^+}^{-1} \exp\left(\frac{1.3F}{RT} E_{2,3}\right) \quad (3.22)$$

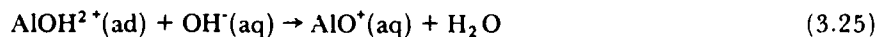
indicating the following rate determining step



Above $\text{pH} = 9$ the rate is given by the equation

$$j_c = k_c {}_3a_{\text{H}^+}^{-2} \exp\left(\frac{1.3F}{RT} E_{2,3}\right) \quad (3.24)$$

with the rate determining step



In both cases a preceding adsorption of OH^- ions from the electrolyte takes place. This is in accordance with the observations made on other oxide covered metal electrodes.

3.4 Stationary metal dissolution current

When the change in oxide thickness has ceased, the electrode has reached steady state. j_{ox} in Equation (3.15) will then be zero and the pd at the oxide electrolyte interface is given by the equation

$$E_{2,3} = \frac{RT}{2F} \ln \frac{k_{\text{ox}}^-}{k_{\text{ox}}^+} + \frac{RT}{2F} \ln {}_2a_{\text{O}^{2-}} + \frac{RT}{2F} \ln {}_3a_{\text{H}^+} \quad (3.26)$$

If this value of E_{23} is introduced into the Equations (3.22) and (3.24), the stationary metal dissolution rate is given by

$$\log j_c(\text{stab}) = \log \left[k_c \left(\frac{k_{ox}^-}{k_{ox}^+} \right)^{1.3} \right] + \frac{1.3}{2} \log a_{O_2} - 0.3 \text{ pH} \quad (3.27)$$

and

$$\log j_c(\text{stab}) = \log \left[k_c \left(\frac{k_{ox}^-}{k_{ox}^+} \right)^{1.3} \right] + \frac{1.3}{2} \log a_{O_2} + 0.7 \text{ pH} \quad (3.28)$$

below and above $\text{pH} = 9$ respectively.

The equations show that if the logarithm of the stationary metal dissolution rate is plotted vs pH, two lines should be obtained, one in solutions below $\text{pH} = 9$ with a slope -0.3 and one with slope 0.7 in solutions above $\text{pH} = 9$.

In order to test this point, experiments were conducted with electrodes anodized to 4 V (SCE) in acetic acid buffered solutions of various pH values. If the electronic conductivity of the formed oxide film is low, only the metal dissolution reaction can proceed when the oxide formation process has ceased. Extreme care was therefore taken not to introduce impurities which could increase the electronic conductivity or weaken the oxide film. The water was therefore deionized and doubly distilled in a quartz still. The first distillation was performed over permanganate in order to oxidize organic impurities. Sometimes it was found necessary to use "suprapur" sodium acetate.

The electrolyte was always 1 M in acetate. Different pH values were obtained by mixing acetic acid and sodium acetate. In the most alkaline solutions sodium hydroxide was added.

The working electrode was made of superpure Al containing $> 99.999\%$ Al. Even though extreme care was taken, parasite reactions often occurred, seen as an increase in the current density instead of a decrease to a constant low value. The parasitic reactions could to some extent be avoided by forming the film to 5 V (SCE) for a short while and then decreasing the potential to 4 V (SCE) where it was allowed to stabilize. Control measurements showed that the same end values of the current density were obtained by the two procedures. In alkaline solutions it was practically impossible to obtain stable values since film breakdown tended to take place.

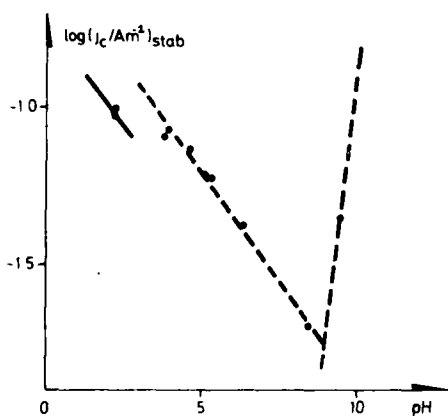


Figure 3.3 The logarithm of the stationary Al dissolution rate at 4 V (SCE) as a function of pH

In Figure 3.3 the results of the experiments are shown in a $\log j_c(\text{stab})$ vs pH plot. As the figure shows, a negative slope is in fact obtained when $\text{pH} < 9$. The slope is approximately -0.15 , *i.e.* smaller than the expected -0.3 , indicating that the values used for z and γ in Equation (3.22) need to be adjusted. The adjustment is most likely to be done on γ , *i.e.* the effective transfer coefficient. By decreasing it from 1.3 to 1.15 , the observed slope can be obtained. The slope in alkaline solutions must then be adjusted accordingly from 0.7 to 0.85 . In Figure 3.3 a line starting from $\text{pH} = 9$ with a slope of 0.85 is drawn. As can be

seen, the line goes through the only point drawn from the experiments in the alkaline range. This indicates that the assumptions are valid. In order to verify the assumptions, however, more experiments with the stationary metal dissolution current are necessary. It must be emphasized that the results are not in conflict with the results obtained in earlier studies (91); only an adjustment of the deduced parameters is necessary. Until more reliable steady state measurements are made, however, such an adjustment is not justifiable.

4 THE INFLUENCE OF POTENTIAL STEPS ON Al-ELECTRODES COVERED WITH THIN OXIDE FILMS

4.1 General

In 1955 Gerisher and Vielstich gave a general description of the potential step method and recommended it for use in electrochemical kinetics (24). The method is now widely used in studying red-ox reactions on active metal electrodes, and the theory is well developed.

The method has also been extensively used in the study of oxide-covered electrodes (15,22,44,45,58,59,73,77,94), but here the theory is much more involved.

On active electrodes the potential step results in a change in the pd at only one interface, i.e. the metal-electrolyte interface. When no diffusion or reaction overvoltage is present, the resulting cd is stable immediately after the step and does not change with time except when the Helmholtz double layer is charged. As pointed out by Vetter (81) and Vielstich (89) the charging time is in the order of 10^{-6} to 10^{-3} s. When diffusion or reaction overvoltage is present, the cd will decrease with time after the step. The decrease is due to a decrease in active species at the metal surface. Immediately after the step, the decrease is usually proportional to the square root of the time, while a proportionality to the inverse square root is observed for longer periods of time.

When the electrode is covered with an oxide film, the transient behaviour changes and a decrease with time occurs even though no diffusion or reaction overvoltage from the electrolyte is present. This has clearly been demonstrated on active and passive iron by Geana *et al* (22). A change in the behaviour is also to be expected since now the pd at two interfaces and across the oxide film are involved.

In the paper describing the general theory of passivity (83) Vetter has also treated the expected result of the potential step.

Using the same notation as in Chapter 2, the electrode potential of an oxide-covered metal electrode can be divided into the following terms

$$E = \varphi(\text{me}) - \varphi(\text{el}) + \Delta \varphi_r = (\varphi(\text{me}) - \varphi'(\text{ox})) + (\varphi'(\text{ox}) - \varphi''(\text{ox})) + (\varphi''(\text{ox}) - \varphi(\text{el})) + \Delta \varphi_r \quad (4.1)$$

where	$\varphi(\text{me}) - \varphi'(\text{ox}) = E_{1,2}$	pd across the metal-oxide interface
	$\varphi'(\text{ox}) - \varphi''(\text{ox}) = E_2$	pd across the oxide
	$\varphi''(\text{ox}) - \varphi(\text{el}) = E_{2,3}$	pd across the oxide-electrolyte interface

The notations are also the same as those used by Vetter and quoted in Figure 4.1.

An electrode which is kept at a certain potential will acquire an oxide film with a certain thickness corresponding to the potential. When the electrode is stable, no further changes in the thickness take place and the oxygen ion exchange between the electrolyte and the oxide will have reached equilibrium. $E_{2,3}$, which then will be the equilibrium potential for the exchange, will then have a certain value, given by pH and the stoichiometry of the oxide surface towards the electrolyte.

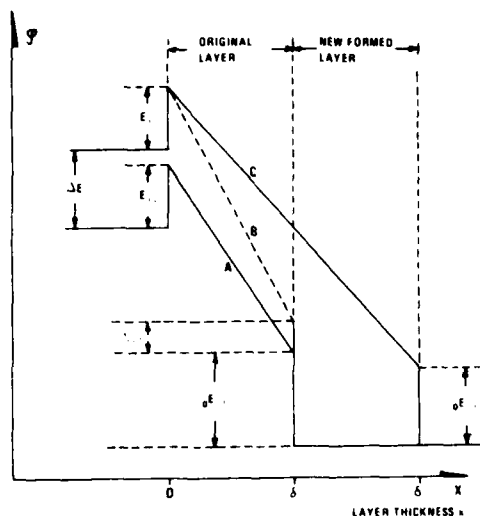


Figure 4.1 Schematic diagram of the potential distribution in an oxide covered metal electrode during a potential step (83)

If both electronic and metallic equilibrium exists between the metal and the oxide surface towards the metal, $E_{1,2}$ will have a fixed value. This is also indicated by Vetter, see Figure 4.1. The thickness of the oxide will then adjust itself in such a manner as to give an electric field in the oxide which is strong enough to maintain an ion transport through the oxide equal to the dissolution rate at the oxide-electrolyte interface (situation A in Figure 4.1).

If now the potential is suddenly increased, the situation denoted B in the figure will arise. Electronic and metallic equilibrium is assumed by Vetter at the metal oxide interface even during the potential step. $E_{1,2}$ will then remain unchanged.

The oxygen ion exchange at the oxide electrolyte interface is no longer at equilibrium and a certain overvoltage $\eta_{2,3}$ will be present. Both the metal dissolution and the oxide formation

rate will therefore increase. The necessary increase in ionic conduction through the oxide is then made possible by the increased electric field across the oxide.

If the electrode potential is kept constant at the new potential, the oxide will increase in thickness. The electric field across the oxide will then decrease and a new equilibrium will be reached for the exchange of oxygen ions between the oxide and the solution. The situation is then the same as that denoted C in Figure 4.1.

The figure indicates that $E_{2,3}$ eventually becomes less than before the step. If, however, the oxide surface has not changed in stoichiometry during the step, the two $E_{2,3}$ values should be equal. The metal dissolution rate should then be equal to the steady state dissolution rate observed before the potential step.

The time which elapses before a new steady state is reached will depend upon the magnitude of the potential step, on the ionic conductivity of the oxide and on the exchange current density of the oxygen-ion exchange reaction. Times in the order of several hours to some days are quite common. In order to change the thickness of the oxide 1 Å, 1.94 C/m^2 has to be consumed. Since the current density during a step is in the order of 0.01 to 0.1 A/m^2 , 20 to 200 s will be necessary for such a change in thickness to take place. 100% current efficiency for the oxygen ion exchange reaction is here assumed. Potential steps lasting less than this, do not therefore normally change the oxide thickness significantly.

4.2 Ion transport

When thick anodic barrier films are present, the stabilization potential will be in the order of 10 to 100 V (SCE). In that case the main part of the total pd lies across the oxide layer and the pd across the metal-oxide and the oxide-electrolyte interface can be neglected. The connection between the ionic current, *i.e.* the sum of the metal dissolution and the oxide formation current, is then according to Gunterschultze *et al* (26) given by the equation

$$j = j_o \exp(B \frac{E - E(0)}{\delta}) \quad (4.2)$$

where $E - E(0)$ -- pd across the oxide film
 δ -- thickness of the oxide film
 B -- constant

See also Chapter 1.

In this equation no time dependency is included. As pointed out by for instance Dignam *et al* (5,73), a time dependent ionic current is observed. According to de Wit *et al* (12), Dignam's equations can be written

$$j = j_o \exp(B_j V + R) \quad (4.3)$$

and

$$\frac{dR}{dt} = (j/q)(B_r V - R) \quad (4.4)$$

where B_j, B_r and q -- constants
 R -- time dependent parameter
 $V = \frac{E - E(0)}{\delta}$ -- the electric field across the oxide
 t -- time

By differentiating Equation (4.3) with respect to t , keeping V constant, it can be shown that

$$\left(\frac{dR}{dt}\right)_V = \left(\frac{d \ln j/j_o}{dt}\right)_V \quad (4.5)$$

i.e. dR/dt is equal to the slope of the $\ln j$ -time curve. When this slope is zero, $B_r V = R$. In that case Equation (4.3) becomes equal to

$$j_{\frac{dR}{dt}=0} = j_o \exp[(B_j + B_r)V] \quad (4.6)$$

which is equal to Equation (4.2) where $B = B_j + B_r$.

When the electrode is stabilized at a certain potential, E_{stab} , Equation (4.6) is valid since $dR/dt = 0$, *i.e.*

$$j_{stab} = j_o \exp[B_j \frac{E_{stab} - E(0)}{\delta} + R_{stab}] = j_o \exp[(B_j + B_r) \frac{E_{stab} - E(0)}{\delta}] \quad (4.7)$$

When the potential suddenly is changed to E , the current will be given by the equation

$$j = j_o \exp[B_j \frac{E_{stab} - E(0)}{\delta} + R] \quad (4.8)$$

where

$$\frac{dR}{dt} = (j/q)[B_r \frac{E - E(0)}{\delta} - R] \quad (4.9)$$

Dividing Equation (4.7) by Equation (4.8), the following equation is derived

$$j/j_{stab} = \exp[(E - E_{stab}) \frac{B_j}{\delta} + (R - R_{stab})] \quad (4.10)$$

where

$$R_{stab} = B_r \frac{E_{stab} - E(0)}{\delta}$$

R is given implicitly by Equation (4.9).

Immediately after the step, R has not been able to change significantly and $R \approx R_{stab}$. In that case Equation (4.10) becomes

$$(j/j_{stab})_{t=0} \approx \exp[(E - E_{stab}) \frac{B_j}{\delta}] \quad (4.11)$$

which shows that also this equation is similar to Equation (4.3), but now $B = B_j$.

When the electrode potential is low, such as in "cathodic corrosion", the situation becomes much more involved. The pd across the oxide may now no longer be dominating and the pd's at the metal-oxide and the oxide-electrolyte interfaces may be a significant part of the electrode potential.

Another complicating factor is that under these circumstances the oxide film is extremely thin and electronic conduction through the oxide may be relatively high. Red-ox reactions like the hydrogen evolution reaction may therefore be dominant. This situation will be discussed further below.

4.3 Electron transport

The total cd can in the general case be written as a sum of two parts, one ionic (j_i) and one electronic (j_e), i.e.

$$j_{tot} = j_i + j_e \quad (4.12)$$

The ionic part can be divided into two parts, i.e. the Al dissolution current j_c and the oxide formation or dissolution current j_{ox} . The electronic cd can only flow if a red-ox couple is present. It has been common practice when studying this current on oxide-covered metals, to use red-ox couples which react in a simple way, i.e. without breaking chemical bonds and without specific adsorption. Such red-ox couples may be

$\text{Fe}(\text{CN})_6^{4-} - \text{Fe}(\text{CN})_6^{3-}$ (35, 67) or $\text{Ce}^{3+} - \text{Ce}^{4+}$ (20, 46). But also more complex reactions, like the oxygen evolution reaction, have been used (87). In the latter case either the reaction



or



was considered to be the rate determining step. At low electrode potentials the hydrogen evolution reaction may easily become the dominating red-ox reaction. Like the oxygen evolution reaction the hydrogen evolution reaction may be divided into several steps, as for instance



As pointed out by Vetter when treating the oxygen evolution reaction, the electron transfer reactions are most probably the rate determining steps in the red-ox reactions on passive metals. In the case of the hydrogen evolution reaction the rate determining step is therefore probably Reaction (4.16). Like Reactions (4.13) and (4.14) for the oxygen evolution reaction, Reaction (4.16) is simply a change from one adsorbed species to another without bond breakings being involved. The situation should therefore be similar to that described by Vetter for the oxygen evolution reaction.

In steady state the pd between the oxide and the electrolyte is still determined by the equilibrium conditions for the oxygen ion exchange between the oxide and the electrolyte. The pd at the interface is therefore not dependent on the electrode potential. The ionic current, *i.e.* $j_{\text{O}^{2-}}$, will therefore be constant and, as pointed out above, independent of the electrode potential. If the electron supply to the interface had been constant, the electronic current should have been constant too. Since this is not the case, the variation in the steady state electronic cd should reflect the electron supply, and only this.

When the stabilization potential is very low, the oxide film becomes extremely thin. In that case electrons may tunnel directly from the metal to the adsorbed species. The electronic current will then depend only on the electrode potential and the thickness of the oxide film, *i.e.* the stabilization potential. The semiconducting properties of the oxide will then play minor roles.

As pointed out by Heusler *et al* (36), such a behaviour can be studied by applying potential steps. The electrode is stabilized in advance at a certain potential in order to obtain a certain thickness. During the step, the oxide thickness can be treated as constant.

Schultze *et al* (67) have pointed out that instead of direct tunnelling, electrons may also be transferred by resonant tunnelling via localized states in the oxide. In that case, semiconducting properties in the oxide may also play a certain role. As pointed out by Heusler *et al* (36), the semiconducting properties may not necessarily be constant during a potential step. Resonant tunnelling, therefore, may give quite a complex picture when potential steps are applied.

On thicker films the probability of tunnelling either directly or via localized states is small. Direct or resonant tunnelling through the space charge barrier is more probable (66). The oxide thickness will then only indirectly play a role. The semiconducting properties will now dominate.

4.4 Electrode capacitance

During a potential step, charging of the space charge layer in the oxide and the Helmholtz layer in the electrolyte will take place. This results in a time dependent charging current. When the oxide is thick and the concentration of donors or acceptors is low, charging of the space charge layer is the dominating process. If virtually no mobile charges are present in the oxide, no space charge layer will be present and the electrode can be treated as a parallel plate condenser where the capacitance increases linearly with the inverse thickness of the oxide film. On the other hand, if the oxide is heavily doped, the capacitance of the Helmholtz layer plays a very important role. Between these extremes, a combination of factors is involved.

Pettinger *et al* (61) and de Gryse *et al* (9) have treated the situation which arises when the oxide is heavily doped and both the space charge and the Helmholtz layer are involved. The total capacitance of the electrode is then given by the equation

$$C^{-2} = 2(e\epsilon_1\epsilon_0N_D)^{-1}E + \left(\frac{\delta_H}{\epsilon_2\epsilon_0}\right)^2 \quad (4.18)$$

where	C	– total capacitance
	N_D	– donor concentration
	e	– elementary charge
	ϵ_1, ϵ_2	– dielectric constants of the oxide and the electrolyte respectively
	ϵ_0	– permittivity of vacuum
	E	– electrode potential
	δ_H	– thickness of the Helmholtz layer

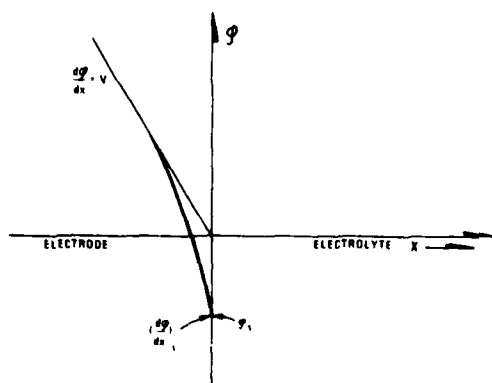


Figure 4.2 Schematic diagram of the potential distribution in the oxide surface towards the electrolyte when a space charge layer and an additional straight field is present in the oxide

The first term on the right-hand side of the equation takes care of the space charge, while the second term takes care of the Helmholtz layer. As the equation shows, the Helmholtz layer becomes more important for higher donor concentrations and lower electrode potentials.

A similar equation can be derived if both a space charge and an additional electric field are present inside the oxide. The model shown in Figure 4.2 can then be used.

When the space charge layer is much thinner than the oxide film thickness, the following limiting conditions can be used

$$\begin{aligned} \text{when } x=0 \quad \varphi &= \varphi_s \text{ and } \frac{d\varphi}{dx} = \left(\frac{d\varphi}{dx}\right)_s \\ \text{when } x \rightarrow \infty \quad \frac{d\varphi}{dx} &\rightarrow V \end{aligned}$$

φ_s is the potential at the oxide surface. When no space charge is present, $\varphi_s = 0$. V is the electric field across the oxide film.

From Poisson's equation we have

$$\frac{d^2\varphi}{dx^2} = -\frac{1}{\epsilon_1\epsilon_0} \rho(x) \quad (4.19)$$

where $\rho(x)$ - space charge density as a function of the distance x

By integration the following equation is derived

$$\int_{x=0}^{x=\infty} d\frac{d\varphi}{dx} = V - \left(\frac{d\varphi}{dx}\right)_s = -\frac{1}{\epsilon_1\epsilon_0} \int_{x=0}^{x=\infty} \rho(x) dx = -\frac{1}{\epsilon_1\epsilon_0} q_{sc} \quad (4.20)$$

where q_{sc} - charge of the total space charge layer

Since

$$\frac{d^2\varphi}{dx^2} \equiv \frac{1}{2} \frac{d}{d\varphi} \left(\frac{d\varphi}{dx}\right)^2 \quad (4.21)$$

the following equation is obtained

$$\int_{x=0}^{x=\infty} d\left(\frac{d\varphi}{dx}\right)^2 = V^2 - \left(\frac{d\varphi}{dx}\right)_s^2 = 2 \int_{\varphi_s}^{\varphi_x \rightarrow \infty} \frac{d^2\varphi}{dx^2} d\varphi = -\frac{2}{\epsilon_1\epsilon_0} \int_{\varphi_s}^{\varphi_x \rightarrow \infty} \rho(\varphi) d\varphi \quad (4.22)$$

which shows that

$$\left(\frac{d\varphi}{dx}\right)_s^2 = V^2 + \frac{2}{\epsilon_1\epsilon_0} \int_{\varphi_s}^{\varphi_x \rightarrow \infty} \rho(\varphi) d\varphi \quad (4.23)$$

If this equation is combined with Equation (4.20), the following equation results

$$q_{sc} = \epsilon_1\epsilon_0 \left(V^2 + \frac{2}{\epsilon_1\epsilon_0} \int_{\varphi_s}^{\varphi_x \rightarrow \infty} \rho(\varphi) d\varphi \right)^{1/2} - \epsilon_1\epsilon_0 V \quad (4.24)$$

The differential capacitance is therefore given as

$$C = \frac{dq_{sc}}{d\varphi_s} = \frac{\rho(\varphi)_s}{\left(V^2 + \frac{2}{\epsilon_1 \epsilon_0} \int_{\varphi_s}^{\varphi_x \rightarrow -\infty} \rho(\varphi) d\varphi\right)^{1/2}} \quad (4.25)$$

The inverse square of this equation is

$$C^{-2} = \frac{V^2}{\rho(\varphi)_s^2} + \frac{2}{\epsilon_1 \epsilon_0} \left[\int_{\varphi_s}^{\varphi_x \rightarrow -\infty} \rho(\varphi) d\varphi \right] \rho(\varphi)_s^{-2} \quad (4.26)$$

When no space charge is present or it is negligible, the second term of the right-hand side of the equation vanishes. Coulomb's law then gives

$$V = (\epsilon_1 \epsilon_0)^{-1} \rho(\varphi)_s \cdot \delta \quad (4.27)$$

where δ — the oxide film thickness

Equation (4.26) will then be

$$C^{-2} = \left(\frac{\delta}{\epsilon_1 \epsilon_0}\right)^2 \quad (4.28)$$

which is the equation for the parallel plate condensor.

When immobile donors are present, the second term in Equation (4.26) becomes equal to the first term in Equation (4.18), which then takes care of the space charge. The situation is therefore very similar to that of a combination of space charge and Helmholtz layer. But the oxide thickness is now involved instead of the thickness of the Helmholtz layer.

The theories on oxide-covered metal electrodes which are cited in this chapter will now be used in the treatment of the results from experiments with potential steps on oxide-covered Al electrodes in aqueous solutions.

4.5 Experimental

The experiments were performed in acetic acid-sodium acetate buffers. Although various pH values were used, the main experiments were performed at pH = 5.20. The acetate concentration was kept constant at 1 molar. Both the acetic acid and the sodium acetate were of AR-quality. The water was double distilled.

The test electrode consisted of a circular Al dish. The aluminium was delivered from Vigeland Metal Refinery and contained $10^{-3}\%$ impurities, mainly magnesium. The dish diameter was 1.4 cm. Before use, the dish was abraded with emery paper, starting with coarse grade, ending with 600 mesh. The dish was etched 10 s in lukewarm 10% NaOH solution, dipped into a 1% acetic acid solution in order to neutralize the NaOH and rinsed in distilled water. The exposed area of the electrode during the experiments was 1 cm^2 .

The counter electrode and the reference electrode were Pt and saturated calomel electrodes, respectively. The reference electrode was kept in a separate compartment

and connected to the cell via a Luggin capillary. The tip of the capillary was close to the surface of the test electrode.

N_2 was continuously bubbled through the electrolyte in order to remove O_2 .

The electrode potential was potentiostatically controlled by means of a potentiostat (PAR mod 173).

The slow transients (up to 5 s) were recorded by an X-Y recorder with time base (HP-7030 AM). A transient recorder (Biomation mod 1015) was used for recording the fast transients.

During the experiments the electrode was allowed to stabilize at a certain potential overnight in order to obtain an oxide film of a certain thickness and composition. From this potential, potential steps of less than 5 s duration were applied to the electrode. After each step the potential was returned to the stabilization potential. When the cd had reached the same value as before the step, a new step was applied to another potential. All experiments were performed at approximately 23°C.

4.6 Results

Figure 4.3 shows examples of current vs time curves after a potential step. As can be seen, fairly stable values are obtained soon after the step, especially when the potential step is small. Immediately after the step a decay in the cd is observed, which might indicate the presence of a charging current. When two curves are compared, resulting from potential steps of the same absolute value but with opposite sign, it can be seen that the decay curves are nearly symmetrical. The stable end current may

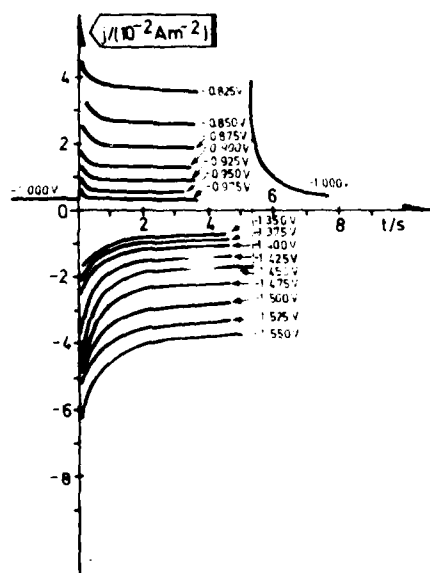


Figure 4.3 Current density-time curves after potential steps in anodic and cathodic directions; potentials against saturated calomel electrodes are given in the figure

Stabilization potential = 1.0 V (SCE), pH = 5.25.

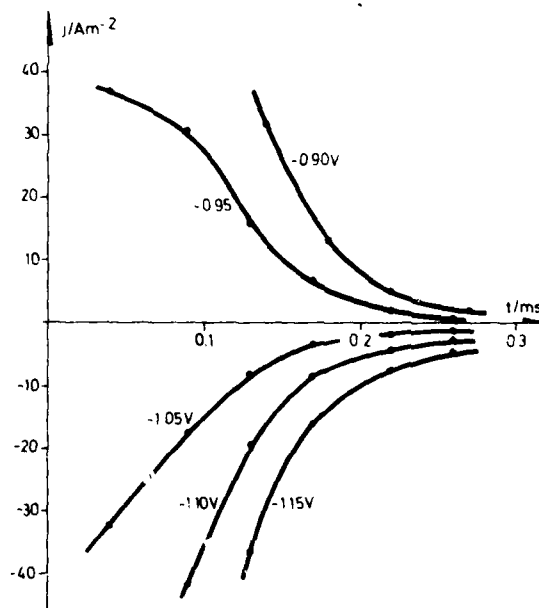


Figure 4.4 Fast current transients immediately after potential steps; potentials against saturated calomel electrode are given in the figure

Stabilization potential = 1.0 V (SCE), pH = 5.25.

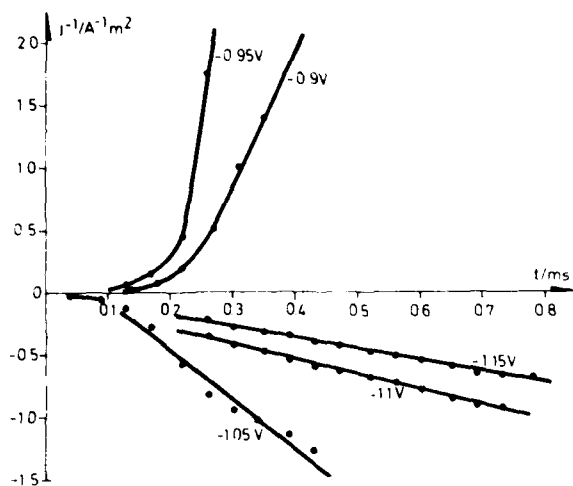


Figure 4.5 The inverse current density vs time for current transients resulting from anodic and cathodic potential steps; potentials against saturated calomel electrode are given in the figure

Stabilization potential = 1.0 V (SCE), pH = 5.25.

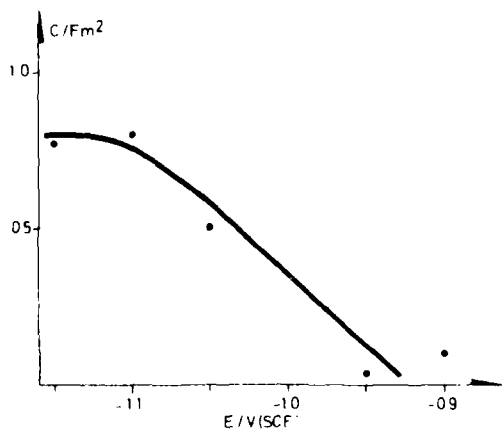


Figure 4.6 The electrode capacity (calculated from the current transients) vs the step potential

Stabilization potential = 1.0 V (SCE), pH = 5.25.

have different values, however. This is to be expected if the decay is due to charging. To obtain further information, potential steps of shorter duration than those described above were created and the decay curves recorded. Figure 4.4 shows examples of cd vs time curves for fast transients. As can be seen, the anodic and cathodic curves have a somewhat different shape, although the magnitude of the cd in both directions is the same.

In Figure 4.5 the results are plotted in an inverse cd vs time plot. As can be seen, straight lines are obtained, except at the very beginning of the transients. Straight lines are also to be expected if a capacitance in series with a resistor is assumed. In that case we have

$$\frac{\Delta E}{j_{ca}} = R + \frac{1}{C}t \quad (4.29)$$

where ΔE = potential step
 j_{ca} = charging cd
 R = series resistance
 C = capacitance
 t = time

The break in the curves in the initial period indicates that Equation (4.29) does not exactly fit the experimental values. A more complicated situation is obviously present. Later on, however, the curves approach a straight line and the slopes of the lines can be used to calculate the capacitance. A connection between the capacity and the step potential can then be obtained, see Figure 4.6. As can be seen from the figure, the capacity of the electrode decreases from approximately 10^{-2} F/m², i.e. the same order of magnitude as the capacity of the Helmholtz layer, down to a very low value. This implies that the oxide layer must play a dominant

ing role in determining the capacity of the electrode. Since the capacity of the electrode can more easily be studied by AC-impedance measurements, the electrode capacity will not be treated further in this chapter, but will be discussed in Chapter 5 where AC-measurements are used. We shall here confine ourselves to pointing out that the decay current observed during potential steps is most probably connected with the capacitance of the electrode and is not due to changes in the electrode reactions.

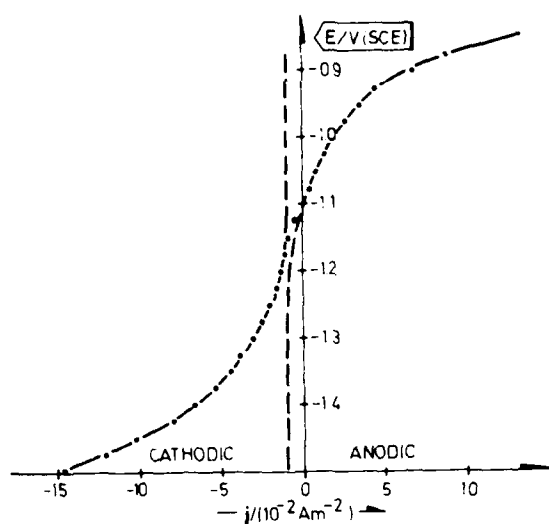


Figure 4.7 The electrode potential vs the step current density (see Figure 4.3)

Stabilization potential -1.1 V (SCE), pH = 5.18.

When the charging current has ceased, the cd becomes stable and will now probably represent either the ionic or electronic current through the oxide film. If the stable cd is plotted vs the potential to which the step is made, *i.e.* the step potential, an S-shaped curve is obtained, see Figure 4.7. The shape indicates that two exponential functions are involved. As can be seen from Figure 4.7, the point of inflection is not at zero cd, but is displaced in the cathodic direction. This displacement is nearly always found and is assumed to be due to a cathodic current flowing in cracks and flaws in the oxide film. If the displaced cd value is subtracted from the total cd and the result is plotted in a Tafel plot, two straight lines are usually obtained, substantiating the suggestion that two exponential functions are involved, see Figure 4.8.

Even if corrections for the displacement are not made, similar curves can be obtained since the difference will only be of importance at low cd values.

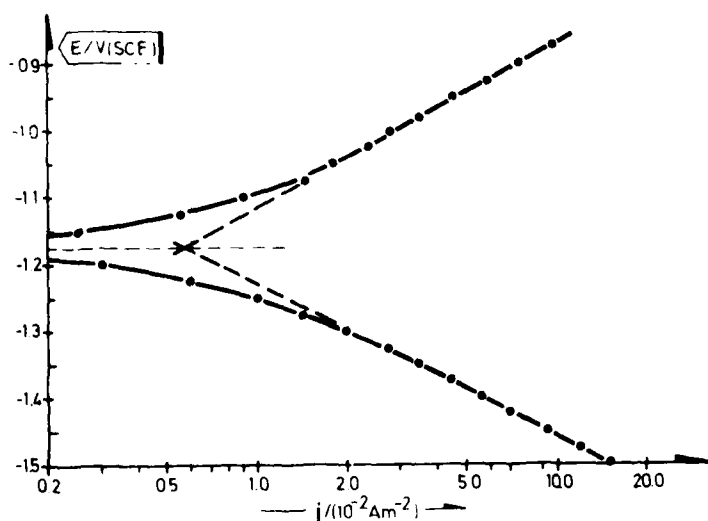


Figure 4.8 Tafel plot of an electrode stabilized at -1.1 V (SCE) pH = 5.18.

It is reasonable to believe that the anodic Tafel line is connected to the ion transport through the oxide. This again is connected to the Al-dissolution and the oxide formation reaction on the oxide surface. Since the oxide formation reaction is at equilibrium when the electrode is at steady state, an extrapolation of the anodic curve to the stabilization potential should give the stable Al-dissolution rate at this potential. In Figure 4.9 this extrapolated cd is plotted *vs* the stabilization potential. As the figure shows, the cd starts at a certain value at high potentials, then decreases towards a minimum at -1.3 V (SCE), whereafter it starts to increase at low potentials. The values given at low potentials may be somewhat uncertain since the cathodic current is dominant at these low potentials and the extrapolation may be difficult to perform. The increasing tendency is, however, clearly seen.

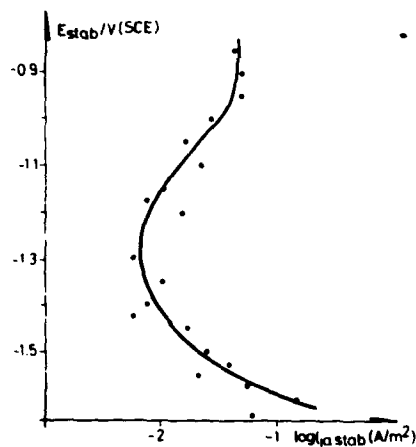


Figure 4.9 The stabilization potential *vs* the logarithm of the anodic current density when extrapolated to the stabilization potential
pH = 5.25

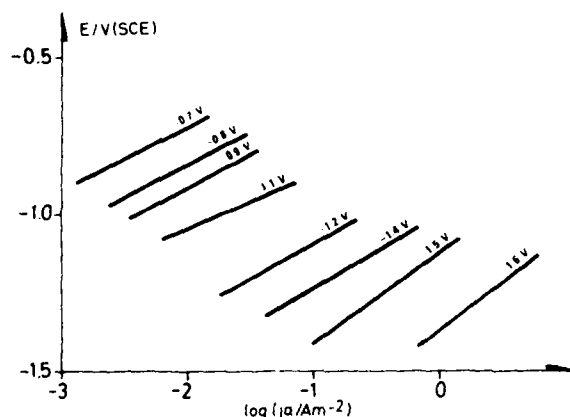


Figure 4.10 Net anodic Tafel curves for electrodes stabilized at different potentials

The stabilization potentials against saturated calomel electrode are given in the figure. pH = 5.25.

In Figure 4.10 anodic Tafel curves representing electrodes stabilized at different potentials are shown. As the figure shows, the curves are displaced towards higher cd values when the stabilization potential is lowered. Since the oxide becomes thinner when the stabilization potential is lowered, such a displacement is also to be expected.

A direct treatment of the Tafel curves may be difficult because the electrode potential is a sum of several potentials. If, however, the curves in Figure 4.10 are read at a certain constant cd , the pd at each interface may, as a first assumption, be treated as constant and the different values obtained must then be due only to differences in the oxide. In Figure 4.11 the electrode potential is plotted *vs* the stabilization potential for different anodic cd values. As the figure shows, the data are quite scattered, primarily due to the varying anodic Tafel slopes. The lines drawn are the best fit from the least square method. In Figure 4.12 the slope of the lines in Figure 4.11 are plotted *vs* the logarithm of the cd at which they are taken. Even though the confidence level is low, the slope of the E_j/E_{stab} lines seems to decrease steadily with decreasing cd .

While the anodic cd is connected to the ionic transport, the cathodic cd is most probably due to electron transport through the oxide. At the oxide electrolyte interface the electrons are consumed by the hydrogen evolution reaction. At low stabilization

potentials the oxide film will be very thin and tunnelling through the film may take place. A connection between the cathodic current at a certain electrode potential and the thickness, *i.e.* the stabilization potential, is then to be expected.

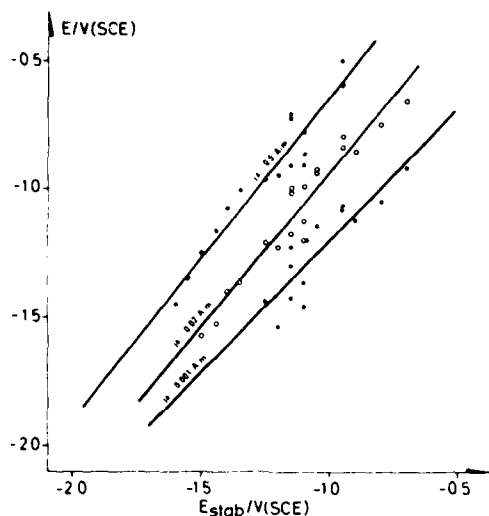


Figure 4.11 The electrode potential at a fixed current density (given in the figure) vs the stabilization potential
pH = 5.25

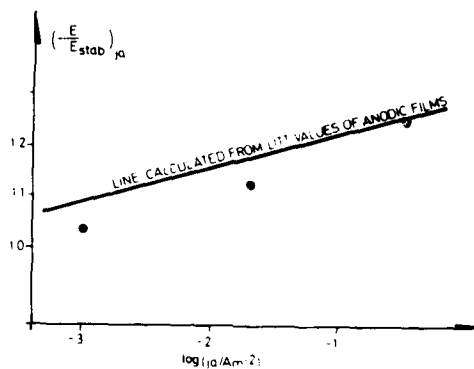


Figure 4.12 The slope of the lines in Figure 4.11 vs the logarithm of the anodic current density
pH = 5.25.

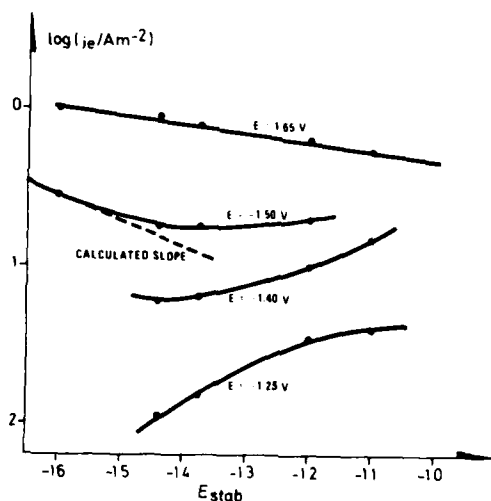


Figure 4.13 The logarithm of the cathodic current density at certain electrode potentials vs the stabilization potential

The electrode potentials against saturated calomel electrode are given in the figure.

In Figure 4.13 the logarithm of the cathodic cd referred to a certain potential is plotted vs the oxide thickness given by the stabilization potential. As the figure shows, a decrease in reaction rate with increasing thickness is observed when the electrode potential is low. At higher potentials this is not observed. Instead some increase is found with increasing thickness. Effects other than direct tunnelling are obviously taking place in the latter case.

The cathodic Tafel slope is also influenced by the stabilization potential. As Figure 4.14 shows, the slope changes from approximately 0.6 V/log unit at high stabilization potentials to nearly 0.1 V/log unit at low potentials. A similar effect is found on changing the pH of the electrolyte, see Figure 4.15. At pH \approx 8.5 the slope is seen to be approximately 0.4 V/log unit, while it is approximately 0.2 V/log unit at pH \approx 4. In this figure the stabilization potential is kept constant.

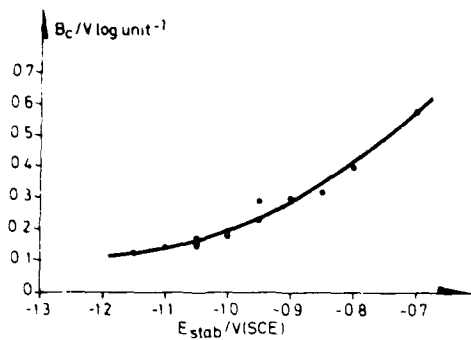


Figure 4.14 The cathodic Tafel slope vs the stabilization potential
pH = 5.20.

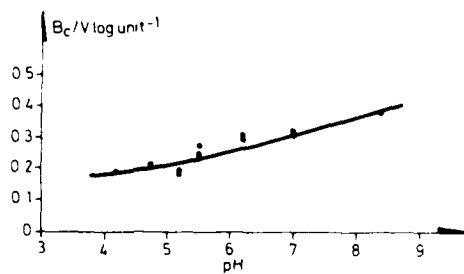


Figure 4.15 The cathodic Tafel slope vs the pH
Stabilization potential = 1.0 V(SCE).

4.7 Discussion

4.7.1 The steady state anodic dissolution rate at low potentials

When the electrode has been stabilized at a certain potential, the oxygen ion exchange reaction at the oxide electrolyte interface has reached equilibrium. The pd at the interface will then have a fixed value, *i.e.* the equilibrium potential of the exchange reaction. It will be independent of the electrode potential but dependent on the pH of the electrolyte and on the oxygen ion concentration in the oxide surface. If these two concentration terms are constant, the pd across the interface will also be constant.

The Al dissolution reaction at the oxide electrolyte interface is also dependent on the pd at the interface. If therefore the aluminium ion concentration in the oxide surface is constant, the dissolution reaction should proceed at a constant rate, independent of the electrode potential. Kaesche (43) has pointed out that such an independent anodic current exists. He has, however, used unbuffered solutions in his experiments. Kunze (47), on the other hand, investigated the Al dissolution in a citrate buffer of pH = 5.0. He states that no such potential independent current could be found. Anderson *et al* (7), examining the leakage current on Al in a tartrate solution of pH = 7 at temperatures from 30°C and up to 70°C, found a potential independent current when the electrode potential was between 50 and 150 V. Below 50 V he found that the cd decreased with decreasing potential.

In Chapter 3 measurements were described of the steady state anodic dissolution rate in acetic acid buffered solutions. In these experiments the potential dependence was also tested by anodizing to 3, 4 and 5 V (SCE). Only a very slight decrease in cd was then found when going to lower stabilization potentials. This tendency may not have anything to do with a real change, but may merely indicate that a completely steady state was not obtained within the time of the experiments.

In Figure 4.9 steady state cd's for stabilization potentials from 0.9 V (SCE) and down to -1.6 V (SCE) are shown. The pH = 5.25 and the results were obtained by extrapolating the anodic Tafel line down to the stabilization potential. If these cd values are compared with those at pH = 5.25 in Figure 3.3, *i.e.* at 4 V (SCE), it can be seen that nearly the same results are obtained when the stabilization potential is more positive than -1.0 V (SCE). This strongly indicates that if there is any potential dependency at all, it is very small when the potential is more positive than

-1.0 V (SCE). At lower potentials a change in the cd is observed, see Figure 4.9. The same change was observed by Kunze (47) and also by Fateev *et al* (19).

Kunze, operating at nearly the same pH as that in Figure 4.9, has obtained cd values which are somewhat higher than those in Figure 4.9. Although the difference is small, it may imply differences in the stabilization time. Since the changes in cd at the end of the stabilization are very slow, Kunze may not quite have reached the end value.

The minimum value obtained by Fateev *et al* is approximately 100 times higher than any obtained by Kunze or by the present author. But since Fateev *et al* used an electrolyte consisting of 1 M KOH, the pH of their solution was quite different. As shown in Chapter 3, a sharp increase in the dissolution rate is to be expected when the pH > 9. In spite of this, the shape of the curves are very similar.

If the assumption of oxygen ion exchange equilibrium is still valid at low potentials, the changing stabilization current at low potentials may be due to either:

- a) A change in the equilibrium potential either as a result of a pH variation or a variation in the surface concentration of O^{2-} ions in the oxide surface
- b) A change in the Al^{3+} concentration in the oxide surface

A change in the pH may occur when the potential is low, since the hydrogen evolution at these potentials is quite rapid and the consumption of H^+ ions may be high. Even in buffered solutions an increase in pH at the oxide surface may therefore occur due to insufficient diffusion of H^+ ions from the bulk electrolyte. As Figure 3.3 in Chapter 3 shows, a decrease in the steady state dissolution rate is to be expected with an increase in pH up to pH=9. This could have explained the decrease in the anodic reaction rate observed in Figure 4.9 when the electrode potential is decreased from -1.0 V (SCE) to approximately -1.25 V (SCE). However, the decrease, which is approximately one logarithmic unit, seems to be too large. Even if the pH had been raised to pH = 9, a decrease due to pH should have been only 0.5 logarithmic units. Effects other than pH must therefore be responsible for the decrease observed in Figure 4.9. The fact that Fateev *et al* (19) observe the same decrease in a 1 M KOH solution supports this conclusion.

The other two possibilities mentioned above, *i.e.* the change in the O^{2-} ion concentration in the oxide surface (which influences the pd) and the change in the Al^{3+} concentration in the surface (which influences the Al dissolution rate) are both related to changes in the oxide stoichiometry. Generally, it is to be expected that the Al^{3+} concentration is increased while the O^{2-} concentration is decreased by lowering the electrode potential. Both these changes should result in an increased Al dissolution rate. This may explain the observed increase in Figure 4.9 at electrode potentials below -1.3 V (SCE), but not the decrease in the range from -1.0 V (SCE) to -1.25 V (SCE). An explanation based on changes in the oxide stoichiometry will, however, require a better knowledge about the potential dependency of these phenomena. Since they are closely connected to the electronic properties of the oxide, it seems reasonable to postpone the discussion until the electronic properties have been dealt with.

4.7.2 Ion transport through the oxide

If ionic conduction through the oxide at low potentials is similar to that at high potentials, the following equation is valid

$$j = j_0 \exp(B \varphi'(\text{ox}) - \delta \varphi''(\text{ox})) \quad (4.30)$$

This equation is equal to Equation (4.2) but $\varphi'(\text{ox}) - \varphi''(\text{ox})$ is used instead of $E - E(0)$ since now the pd across the oxide may not be the dominating part of the electrode potential.

From Equation (4.1) the pd across the oxide is given as

$$\varphi'(\text{ox}) - \varphi''(\text{ox}) = E - [\varphi(\text{me}) - \varphi'(\text{ox}) - (\varphi''(\text{ox}) - \varphi(\text{el})) + \Delta\varphi_r] \quad (4.31)$$

The thickness (δ) of the oxide film is related to the stabilization potential by

$$\delta = U(E_{\text{stab}} - E(0)) \quad (4.32)$$

where U — anodizing ratio ($\sim 13 \text{ \AA/V}$ (30))*
 $E(0)$ — electrode potential when no field exists across the oxide film

If Equations (4.31) and (4.32) are introduced into Equation (4.30), the following equation is derived

$$j = j_0 \exp \left\{ \frac{B}{U} \frac{E - [\varphi(\text{me}) - \varphi'(\text{ox})] - [\varphi''(\text{ox}) - \varphi(\text{el})] - \Delta\varphi_r}{E_{\text{stab}} - E(0)} \right\} \quad (4.33)$$

or

$$E = [\varphi(\text{me}) - \varphi'(\text{ox})] + [\varphi''(\text{ox}) - \varphi(\text{el})] + \Delta\varphi_r + \frac{U}{B} [E_{\text{stab}} - E(0)] \ln j / j_0 \quad (4.34)$$

When this equation is differentiated with respect to E_{stab} , the following equation results

$$\frac{dE}{dE_{\text{stab}}} = \frac{d[\varphi(\text{me}) - \varphi'(\text{ox})]}{dE_{\text{stab}}} + \frac{d[\varphi''(\text{ox}) - \varphi(\text{el})]}{dE_{\text{stab}}} + \frac{U}{B} \left[\ln j / j_0 + (E_{\text{stab}} - E(0)) \frac{d \ln j / j_0}{dE_{\text{stab}}} \right] \quad (4.35)$$

If the electrode potential (E) is read at a certain anodic cd (j_a) for different stabilization potentials, Equation (4.35) is reduced to

$$\left(\frac{\partial E}{\partial E_{\text{stab}}} \right)_{j_a} = \frac{U}{B} \ln(j_a / j_0) \quad (4.36)$$

since the pd's at both interfaces are constant for a constant cd.

* Strictly speaking, the anodizing ratio is dependent on the steady state dissolution rate and thereby on pH. The anodizing ratio referred to (13 \AA/V) is found in neutral solutions. At pH = 5.25 a somewhat lower anodizing ratio is to be expected. Since the dissolution rate at pH = 5.25 is only slightly higher than in neutral solutions, the expected difference in anodizing ratio is probably smaller than the error connected to the anodizing ratio.

If now the values

$$j_0 = 3.62 \cdot 10^{-19} \text{ A/m}^2$$

$$B = 4.25 \cdot 10^{-8} \text{ m/V}$$

found by Gunterschultze *et al* (26) at high anodic potentials are introduced into Equation (4.36) together with the anodizing ratio $U = 13 \text{ A/V}$ found by Hass (30), $(dE/dE_{\text{stab}})j_a$ as a function of j_a can be calculated.

In Figure 4.12 these calculated values are shown together with those found experimentally at low potentials. As can be seen from the figure, the deviation between the calculated and the experimental values is very small and easily within the experimental error. It seems therefore beyond doubt that the mechanism for ionic conduction found at high anodic potentials is valid also at low potentials, *i.e.* in the "cathodic corrosion" area. It means also that the connection between the stabilization potential and the oxide thickness, given by the anodizing ratio, is still valid. If therefore $E(0)$ could be determined, the oxide thickness could be estimated for each stabilization potential.

From Equation (4.34) it can be seen that when E_{stab} is equal to $E(0)$, the slope of E vs j_a becomes equal to the Tafel slope of the active Al dissolution reaction. Since the cd 's used to plot the curves in Figure (4.11) are very small, it is likely that these cd 's are smaller than, or at most equal to, the exchange current density of the active dissolution reaction. In that case the variation in E with j_a is likely to be small, indicating that when E_{stab} is equal to $E(0)$, E will be nearly independent of j_a . As Figure 4.11 shows, an extrapolation of the curves to a common point seems possible. Taking into account the experimental error, the potential at this point seems not to deviate greatly from the thermodynamic potential -2.027 V (SCE) calculated from Equation (2.26). This may also be taken as a verification of the assumptions made in Chapter 2. It also means that since the stabilization potentials used in this work have values between -0.7 and -1.6 V (SCE) , the oxides will have thicknesses between approximately 5.5 and 17.7 \AA .

4.7.3 Electron transport

In the previous section it was concluded that the electrodes in the "cathodic corrosion" range are covered with extremely thin oxide films. For such thin films, electron tunnelling will take place through the oxide and, at least for the thinnest oxides, a connection between the oxide thickness and the electron transport is to be expected (36,46,66,87).

The hydrogen evolution reaction is dependent on the electron transport through the oxide. This reaction may therefore be used as a measure of the electron transport. The electron supply must then be part of the rate determining step. Such a step may be the reduction of adsorbed H^+ ions to H atoms. The situation will then be similar to that assumed for the oxygen evolution reaction by Vetter *et al* (87). In their case the rate determining step was assumed to be the oxidation of adsorbed OH^- ions to adsorbed OH or adsorbed O^{2-} ions to adsorbed O^- . Since the electron transport is to a great extent hampered by the oxide film, such steps may well be rate determining.

When electron tunnelling from the metal to the adsorbed ions occurs, the reaction rate will be given by

$$\log j_e = A(E) \frac{\delta}{\delta_0} \quad (4.37)$$

(see ref (87))

- where j_e — rate of the hydrogen evolution reaction
 $\Lambda(E)$ — potential dependent term, independent of the oxide thickness
 δ — thickness of the oxide
 δ_0 — potential dependent constant

According to (87), δ_0 is defined by

$$\delta_0 = \frac{2.3h}{4\pi \sqrt{2}mc\Delta E_b(E)} = \frac{2.26}{\sqrt{\Delta E_b(E)}[\text{eV}]} \text{ [Å]} \quad (4.38)$$

- where h — Planck constant
 m_e — effective mass of electron
 $\Delta E_b(E)$ — mean barrier height in the oxide

Combining Equations (4.32) and (4.37), the following equation is obtained

$$\log j_e = \left[\Lambda(E) + \frac{E(0)U}{\delta_0} \right] - \frac{U}{\delta_0} E_{\text{stab}} \quad (4.39)$$

- where $E(0)$ — potential when no field exists in the oxide
 U — anodization ratio
 E_{stab} — stabilization potential

For constant electrode potentials the terms inside the bracket on the right-hand side of Equation (4.39) will be constant. In that case a plot of the logarithm of the cathodic cd vs the stabilization potential should give a straight line. U/δ_0 will be the slope of the line.

In Figure 4.13 the logarithm of the experimental cd's for different electrode potentials are plotted vs the stabilization potential. As can be seen, only the most negative electrode potential plotted gives a straight line. The slope of the line indicates an δ_0 value of 23 Å when an anodization ratio of $U = 13 \text{ V/V}$ is used. This δ_0 value corresponds to a value of $\Delta E_b(E) = 0.01 \text{ eV}$, which is very low compared to the value found for other red-ox reactions on for instance oxidized Pt (46).

The energy barrier $\Delta E_b(E)$ can, according to Vetter *et al* (87), be divided into a potential dependent and a potential independent part, i.e.

$$\Delta E_b(E) = \Delta E_b^0 + \frac{E - E(0)}{2}e \quad (4.40)$$

- where ΔE_b^0 — energy barrier when no field is present in the oxide
 e — elementary charge
 E — actual electrode potential
 $E(0)$ — electrode potential when no field is present

From this equation the potential independent energy barrier can be calculated.

When the data from the upper curve in Figure 4.13 are used, *i.e.*

$$\begin{aligned}\Delta E_b(E) &= 0.01 \text{ eV} \\ E &= 1.65 \text{ V (SCE)} \\ E(0) &= 2.03 \text{ V (SCE)}\end{aligned}$$

the potential independent barrier, $\Delta E_b^0 = 0.18 \text{ eV}$ is arrived at.

This value can now be used to calculate the expected slope of the other curves in Figure 4.13. When for instance 1.50 V (SCE) is used for E instead of 1.65 V (SCE) , the energy barrier $\Delta E(E)$ becomes equal to 0.09 eV , giving an expected slope for the next upper curve equal to 1.73 V^{-1} . The broken line in the figure is drawn with this slope. As can be seen, the line might well be the asymptote of the curve for low stabilization potentials. The curve deviates, however, remarkably from the line at higher stabilization potentials. The remaining curves in Figure 4.13 show no sign of the expected tunnelling effect. Other mechanisms are obviously then dominating. The reason might be that the assumption of electron transport being rate determining is no longer valid. If it is still valid, the electrons may now tunnel from for instance the conduction band in the oxide. Dogonadze *et al* (16) have pointed out that if the potential-dependent part is the dominating part of the total energy barrier, such a tunnelling is favorable. The above calculated energies show that this will certainly be the case.

If electron transport is not rate determining, the adsorption rate and the concentration of adsorbed H^+ ions on the oxide surface may determine the rate of the hydrogen evolution reaction. Both these factors are influenced by pH. Information on such rate determining steps should therefore be gained by comparing results from experiments where pH was changed, with experiments where pH was kept constant while other parameters were varied. In Figures 4.14 and 4.15 the cathodic Tafel slope is plotted vs the stabilization potential and the pH, respectively. Since the stabilization potential determines the oxide thickness, Figure 4.14 really shows the Tafel slope vs the thickness. As can be seen, the slope increases with increased oxide film thickness.

Contrary to Figure 4.14, where the pH is kept constant, the stabilization potential in Figure 4.15 is kept constant and the pH is varied. This variation may act in two ways.

First of all, a pH variation will change the degree of adsorption. Secondly, an increase in pH will cause a lowering of $E(0)$, *i.e.* the electrode potential where no field exists across the oxide, see Equation (2.26). The difference $E - E(0)$, which determines the oxide thickness, will therefore be changed even though the electrode potential is kept constant. A plot of the transfer coefficient vs the thickness can therefore also in this case be made. If the data in Figures 4.14 and 4.15 give the same relationship between the transfer coefficient and the calculated thickness, the thickness variation and thereby the electron transfer will most probably be rate determining.

In Figure 4.16 such a thickness plot is shown. As can be seen, the results are virtually the same. A somewhat lower transfer coefficient seems to be obtained when pH is used as basis for the thickness calculations, see the figure. The difference is, however, very small and probably not significant. The results in the figure therefore give a strong indication that the thickness, and thereby the electron transfer, still plays the dominating role, even in the thickness range 10 to 20 Å. Since the previous results indicate that direct tunnelling from the metal is only significant for low potentials, tunnelling from positions in the oxide seems to be responsible for the electron transport.

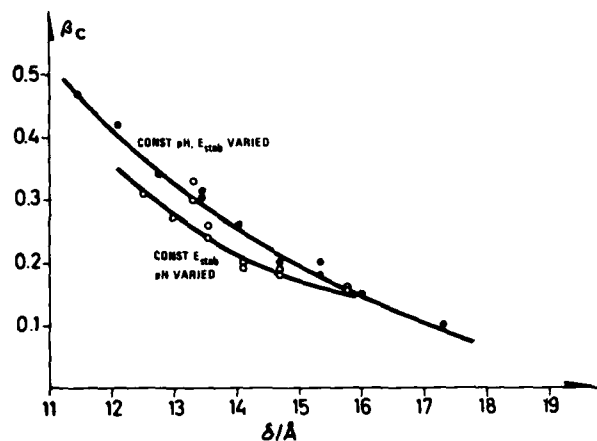


Figure 4.16 The cathodic transfer coefficient vs calculated oxide film thickness

- pH = 5.20, E_{stab} varied
- E_{stab} = -1.0V(SCE) pH varied

fer. But even such a tunnelling seems to depend on the total oxide thickness.

Further treatment of the subject will, however, be very speculative without more detailed knowledge about the electronic structure of the oxide. The subject will therefore be discussed further in Chapters 5 and 6.

5 THE CAPACITANCE OF THE Al ELECTRODE

5.1 General

Capacity measurements are widely used for studying passive films. The use of the method can roughly be divided into three main areas:

- a) Determining the porous structure of the oxide film
- b) Determining the thickness of the film
- c) Determining the electronic structure

Capacity measurements combined with resistivity measurements at different frequencies have been used by Libsch and Devereux for studying anodized Al (50,51). By assuming some electrical analog equivalent circuits they found the method well suited for the study of pore formation in the oxide and the formation of hydrous layers upon the barrier layer. Since such phenomena are not particularly covered in the present work, this subject will not be treated further here.

When no mobile charges are present in the oxide film, a space charge layer will not be formed. The electric field will then go straight through the oxide. The oxide can then be treated as a pure dielectric and the electrode as a parallel plate condenser.

According to the equation for this condenser, the oxide thickness will be inversely proportional to the electrode capacity; *i.e.*

$$C = \frac{\epsilon\epsilon_0}{\delta} \quad (5.1)$$

where	C	— capacitance
	δ	— oxide film thickness
	ϵ	— relative dielectric constant of the oxide
	ϵ_0	— permittivity of vacuum

The equation is well suited for calculating the oxide thickness from the capacity. Such calculations have been used on nearly all passive met ls. Thickness measurements on anodized Al based on the capacity are reported for instance by Smith (69), McMullen *et al* (52) and Videm (88).

Smith (69) has plotted the inverse capacitance *vs* the formation voltage for different frequencies (0.2 to 10 kHz). He finds a row of nearly parallel lines with the high frequency line (10 kHz) on the top and the low frequency line (0.2 kHz) on the bottom. The difference between the 2 kHz line and the 0.2 kHz line is, however, very small, indicating only a weak frequency dependency in this range. A similar result is obtained by Videm (88) in the range 50 to 500 Hz.

In order to determine the oxide thickness, the relative dielectric constant of the oxide has to be known. In the literature, values for this constant seem to vary somewhat. Smith used the value 8.7 given by van Geel *et al* (75), McMullen *et al* (52) used the value 8 and Videm gives a value of 12.5 when no corrections for roughness of the electrode are made. He also cites Harkness *et al* (28) and Vermilyea (78), giving values of 10.2 and 10.5 respectively when corrected for the roughness.

If mobile charges are present in the oxide, a space charge layer will be built up. This will cause a decrease in the straight field dealt with above and it may eventually vanish. In that case the potential does not change in the interior of the oxide. The capacity of the electrode is then given by the equation (24)

$$C^2 = \frac{1}{2} \epsilon \epsilon_0 [\rho(\varphi_s)]^2 \left[\int_0^{\varphi_s} \rho(\varphi) d\varphi \right]^{-1} \quad (5.2)$$

where $\rho(\varphi_s)$ — density of charge in the oxide surface
 $\rho(\varphi)$ — density of charge in the oxide where the potential is φ relative to the interior

When the mobile charges are negative and the immobile are positive, the oxide behaves as an n-type semiconductor. For large anodic potentials, i.e. $\varphi_s \gg \frac{kT}{e}$, the Mott-Schottky approximation can be used (11), i.e.

$$C^2 = \frac{e^2 N_D \epsilon \epsilon_0}{2kT} \left[-f + \ln f - \frac{e}{kT} \varphi_s \right]^{-1} \quad (5.3)$$

where e — elementary charge
 N_D — donor concentration
 k — Boltzmann constant
 T — absolute temperature
 f — fraction of donors that are ionized in the bulk oxide

A plot of the inverse square of the capacity vs the electrode potential will in that case give a straight line. The slope of the line will be a measure of the donor concentration.

An extrapolation of the line to $C^{-2} \rightarrow 0$ should give the electrode potential where φ_s is equal to $\frac{kT}{e} [-f + \ln f]$. When the donors are completely ionized, $f = 1$ and $\varphi_s = -\frac{kT}{e}$ for the extrapolated value. By subtracting kT/e from the extrapolated electrode potential, the electrode potential where $\varphi_s = 0$ is found. This electrode potential is called the flat band potential.

The method has been extensively used to determine the donor concentration and the flat band potential on several oxide films on metals other than Al.

For instance, Heusler *et al* have used the method to study the oxide films on Nb (32) and Ti (1). On both these oxides they found that the donor concentration was inversely proportional to the square root of the oxide thickness. On Nb they also found that the flat band potential increased with increasing oxide thickness.

Stimming *et al* (70) used the capacity measurements to determine the flat band potential and the donor concentration on passive Fe. While Heusler *et al* (1, 32) used relatively thick oxides (150 to 280 Å), Stimming *et al* (70) used oxide films in the order of 10 to 30 Å on Fe. Stimming *et al* separated the capacitance vs potential curve

into three parts. In the first part, which extended from 0 to 0.5 V, the capacitance decreased with increasing potential. In the second part, *i.e.* between 0.5 and 1.0 V it was constant. Above 1.0 V the capacitance increased with increasing potential. In the constant part the capacity was shown to be related to the oxide thickness and a proportionality between the inverse capacity and the thickness was found. The Mott-Schottky relationship was applied to the first part, *i.e.* the region where the capacity decreased with increasing potential. By assuming a dielectric constant $\epsilon = 12$, a donor concentration in the order of $1.5 \cdot 10^{26} \text{ m}^{-3}$ was found for a 27 Å thick film. The donor concentration was found to increase with a decrease in the film thickness. The flat band potential was also found to be a function of the thickness. For the 27 Å thick film the flat band potential was -70 mV, while -150 mV was found for a 17 Å thick film.

The increase in capacity at high potentials was explained as due to a contribution from the valence band and creation of holes.

In many respects the work of Stimming *et al* (70) on Fe is related to the present work on Al. The two oxides both have the disordered γ -structure and the thickness ranges studied are similar (~ 5 to 30 Å). On one point, however, a difference is to be expected. While Stimming *et al* observed a contribution from the valence band, no such contribution is likely to be present on Al since the band gap here is much higher (1–1.6 eV for $\gamma\text{-Fe}_2\text{O}_3$ (70) and 5.2 eV for $\gamma\text{-Al}_2\text{O}_3$ (72)).

5.2 Experimental

The capacity measurements were performed with an Al-electrode (99.999% Al) in an electrochemical cell containing 1 molar acetic acid – sodium acetate buffer of pH = 5.20. Both the acetic acid and the sodium acetate were of AR-quality. The water was deionized and double distilled over permanganate in a quartz still.

During the experiments the electrode potential was potentiostatically controlled by a potentiostat equipped with an alternating current measurement device (Tacussel type PRG3). With this instrument the potential could easily be switched from one value to another and back again. A small alternating potential with 2 mV amplitude could be superimposed on the main potential and the resultant current be measured, both that in phase with the alternating potential and that 90° out of phase. From these current components the series capacitance was calculated. The frequency could be varied from 3 to 3000 Hz, but only 1000 and 3000 Hz were used since the frequency dependency according to Smith (69) and Videm (88) here is small and the results could be compared with other capacity measurements.

Sometimes the Al-electrode was electropolished in an alcoholic perchlorate solution and anodized to 5 V in a 3% ammonium tartrate solution prior to the experiments. This should assure an even 92 Å thick oxide film.

Usually, however, the electrodes were abraded with emery paper, starting with coarse grade, ending up with 600 mesh. Then they were etched for 10 s in lukewarm 10% NaOH solution, dipped into a 1% acetic acid solution in order to neutralize the NaOH and rinsed in distilled water. They were then kept in the cell containing the acetate buffer overnight at a certain potential, *i.e.* the stabilization potential.

N₂ was continuously bubbled through the electrolyte in order to remove O₂. The cell and the reference electrode (saturated calomel electrode) were kept in a thermostated vessel at $25 \pm 0.5^\circ\text{C}$.

5.3 Results

When the electrode covered with the 92 Å thick oxide film is immersed into the electrolyte and kept at -1.1 V (SCE), a pronounced increase in capacity with time is seen. The capacity is, however, virtually potential independent, even after 28 hours of immersion, see Figure 5.1. The potential dependency was tested by applying potential steps of short duration (~ 10 s). Between each step the potential was returned to the stabilization potential (-1.1 V (SCE)) in order to ensure that no irreversible changes had occurred. The range covered was from -1.7 to 0 V (SCE).

After approximately 30 hours a small potential dependency was observed, see curve 7 in Figure 5.1. From now on, the potential dependency became even stronger, as also shown by curve 8 and 9 in the figure.

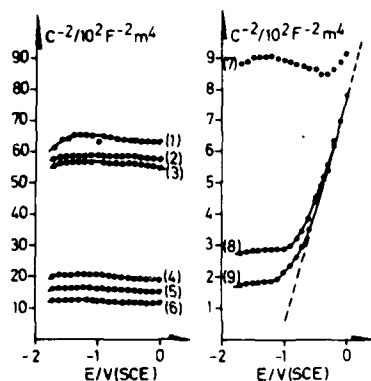


Figure 5.1 The inverse square of the capacity vs the electrode potential

Film formed at 5 V (SCE) and then kept at -1.1 V (SCE) for: i) 1 hours, ii) 3.25 hours, iii) 6 hours, iv) 24 hours, v) 26 hours, vi) 28 hours, vii) 31 hours, viii) 48 hours and ix) 53 hours.

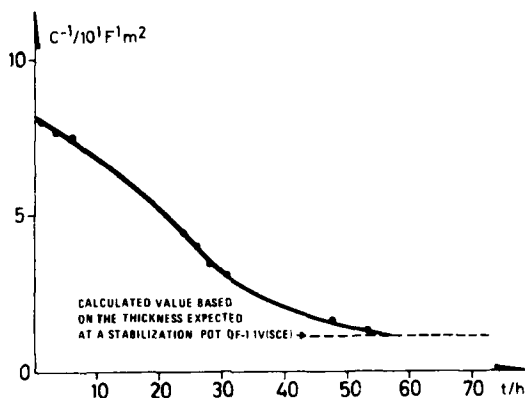


Figure 5.2 The inverse value of the potential independent capacity vs time at -1.1 V (SCE) after being anodized to 5 V (SCE)

In Figure 5.2 the inverse value of the potential independent capacity is plotted vs time. As the figure shows, the inverse capacity decreases steadily from approximately $87 \text{ m}^2/\text{F}$ at zero time to $13 \text{ m}^2/\text{F}$ after 53 hours.

By treating the electrode as a parallel plate condenser, the oxide thickness can be calculated using Equation (5.1), i.e.

$$\delta = \epsilon \epsilon_0 C^{-1} \quad (5.1)$$

where

C	— measured capacity in F/m^2
δ	— oxide thickness
ϵ	— 12 (relative dielectric constant)
ϵ_0	— $8.85 \cdot 10^{-12} \text{ F}/\text{m}$ (permittivity of vacuum)

The calculated oxide thickness was at the beginning $8.81 \cdot 10^{-9} \text{ m}$ or 88.1 Å, which corresponds well to the expected 92 Å. After 53 hours the calculated oxide thickness was found to be $1.38 \cdot 10^{-9} \text{ m}$ or 13.8 Å. If the potential of zero field, $E(\text{O})$, is

-2.03 V (SCE), see chapter 2, the potential difference across the oxide should be 0.93 V when the electrode is stabilized at -1.1 V (SCE). This should give an expected steady state thickness of 12 Å, provided that the anodizing ratio is 13 Å/V. As can be seen, this value corresponds well to the thickness calculated on the basis of the potential independent capacity after 53 hours.

The experiment indicates that there is a close connection between the potential independent capacitance and the oxide thickness. It also indicates that when a relatively thick oxide is kept at a low potential for some time, the oxide thickness will decrease and probably reach a value corresponding to the new low potential. The oxide dissolution may, however, take several days to reach the final stage.

The potential dependent capacity seems to approach a straight line in the C^{-2} vs E plot, see Figure 5.1. Contrary to the potential independent capacity, the line seems to be nearly independent of time. This indicates that changes in the space charge layer and thereby the donor concentration are hardly affected at all by the oxide thickness in this experiment.

If the Mott-Schottky approximation is used, *i.e.* Equation (5.3), the slope of the line gives a donor concentration $N_D \approx 1.5 \cdot 10^{26} \text{ m}^{-3}$. An extrapolation of the curves in Figure 5.1 to zero, indicates a flat band potential in the vicinity of -1 V (SCE).

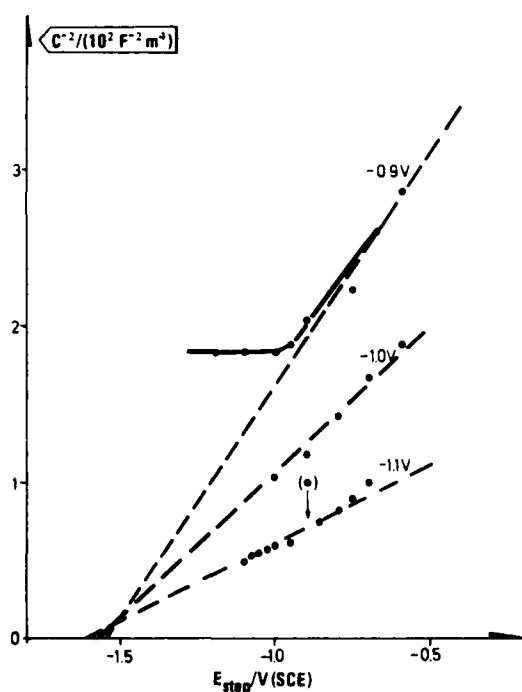


Figure 5.3 *The inverse square of the capacity vs the step potential*

The curves represent electrodes stabilized at different potentials. The stabilization potential vs saturated calomel electrode is given in the figure.

The capacity vs the potential was also measured on abraded and etched electrodes. Prior to the measurements, the electrodes were allowed to stabilize at a certain potential overnight in the electrolyte. Figure 5.3 shows the result of these measurements in Mott-Schottky plots. As can be seen, the stabilization potential has a pronounced effect on the result. When the electrode is stabilized at -0.9 V (SCE), a curve similar to that shown in Figure 5.1 is obtained, see the upper curve in Figure 5.3. When the potential independent part of the curve is used to calculate the oxide thickness, an oxide thickness $\delta = 14.3$ Å is obtained. Since the potential difference across the oxide is 1.13 V at this stabilization potential, the anodization ratio of 13 Å/V gives an expected oxide thickness of 14.69 Å. This correspondence gives a strong indication that the potential independent part of the capacity is still strongly related to the oxide thickness. It further shows that the oxide thickness is related to the stabilization potential, as also indicated in previous chapters.

When the Mott-Schottky approximation is used on the potential dependent part of the curve representing the electrode stabilized at -0.9 V (SCE), a donor concentration

$N_D \approx 2.95 \cdot 10^{26} \text{ m}^{-3}$ is obtained. This concentration is approximately twice that found in the oxide formed at 5 V (SCE) but then kept at -1.1 V (SCE). The flat band potential of the electrode seems also to be displaced towards more negative potentials when compared with the 5 V oxide.

When the electrode is stabilized at lower potentials than -0.9 V (SCE), the potential independent part of the capacity assumes a higher value, *i.e.* C^{-2} becomes lower, and may nearly vanish. An increase in capacity is certainly to be expected since the oxide probably becomes thinner. The increase is, however, much stronger than would be expected if only the thickness had changed. The oxide thickness is obviously not the only factor which determines the potential independent capacity of these electrodes.

When the Mott-Schottky approximation is used on the potential dependent part of the capacity, it is seen that the donor concentration increases steadily with decreasing stabilization potential when a constant dielectric constant is assumed. If the stabilization potential is -1.1 V (SCE), the donor concentration is found to be $1.13 \cdot 10^{27} \text{ m}^{-3}$ provided that a dielectric constant $\epsilon = 12$ is used. A similar donor concentration was also found by Schultze *et al* (67) on oxide covered iron. This is an extremely high donor concentration. It is nearly 10 times greater than that obtained when the 92 Å thick oxide was thinned down.

This shows that even though the stabilization potential was the same in the two cases, and equal thickness was to be expected, the two electrodes behaved in quite different ways. A thick oxide film which is thinned down seems to assume different properties than oxide films formed directly on etched electrodes. The difference may, however, be a matter of reaching complete steady state or not, and as pointed out by Vetter (83), stoichiometric changes may take time.

5.4 Discussion

In the preceding section it has been shown that capacity measurements can give information on both the oxide thickness and the space charge layer in the oxide. The potential independent part of the capacity curve can be treated as if the oxide were a dielectric. The Mott-Schottky approximation can, on the other hand, be used on the potential dependent part. A similar dualistic treatment has also been made by Schultze *et al* (67) when treating the capacity on oxide covered iron electrodes. The question is why this can be done.

In Chapter 4 it was shown that when both a space charge layer and an electric field were present inside the oxide, the inverse square of the capacity could be written as

$$1/C^2 = V^2/\rho_s^2 + \frac{2}{\epsilon\epsilon_0\rho_s^2} \int_{\varphi_s}^{\varphi_x \rightarrow -\infty} \rho d\varphi \quad (4.25)$$

or

$$\frac{\rho_s^2}{C^2} = V^2 + \frac{2}{\epsilon\epsilon_0} \int_{\varphi_s}^{\varphi_x \rightarrow -\infty} \rho d\varphi \quad (5.2)$$

where ρ_s — charge density of the oxide at the surface towards the electrolyte
 C — capacity

where	V	— straight electric field inside the oxide
	ϵ	— dielectric constant of the oxides
	ϵ_0	— permittivity of vacuum
	ρ	— space charge density in the oxide
	x	— distance from the oxide-electrolyte interface, positive when going from the oxide to the electrolyte
	φ	— potential relative to the oxide surface towards the electrolyte when no space charge is present

When only donors and electrons are present, the space charge density is given by the equation

$$\rho = eN_D - en \quad (5.3)$$

where	e	— elementary charge
	N_D	— donor concentration
	n	— electron concentration

According to Gerisher (24) the electron concentration is given by the equation

$$n = N_C \exp[-(E_C - E_F - e\varphi)/kT] \quad (5.4)$$

where	N_C	— effective density of states
	E_C	— energy level corresponding to the bottom of the conduction band
	E_F	— Fermi level
	k	— Boltzmann constant
	T	— absolute temperature

When $\varphi = 0$, i.e. the potential equals that existing at the oxide surface when no space charge is present, Equation (5.4) becomes

$$n^0 = N_C^0 \exp[-(E_C - E_F)/kT] \quad (5.5)$$

which combined with Equation (5.4) gives

$$n = n_0 \exp(e\varphi/kT) \quad (5.6)$$

If the electrode is stabilized at a certain potential, the ion transport through the oxide will reach steady state. In that case the ions will be transported through the oxide at the same rate, indicating that the field strength is nearly constant. Virtually no space charge layer can then be present. A small but insignificant space charge layer may be present if the stoichiometry of the oxide changes, but since the devi-

ation from a stoichiometric oxide probably is small, it is likely that this will play a minor role. In that case Equation (5.3) shows that $N_D = n$.

Since the potential $\varphi = Vx$ when no space charge is present, the donor concentration is given by Equation (5.6) when Vx is introduced for φ and N_D for n , i.e.

$$N_D = N_D^0 \exp(exV/kT) \quad (5.7)$$

where N_D^0 is the concentration of donors in the oxide surface towards the electrolyte when no space charge is present.

If we assume that during a potential step only the electrons respond, i.e. the donors are virtually immobile, Equation (5.7) will still be valid for the donors. The electrons will, however, change according to Equation (5.6). Equation (5.3) can then be written as

$$\rho = eN_D^0 [\exp(exV/kT) - \exp(e\varphi/kT)] \quad (5.8)$$

which gives the space charge density during a potential step.

The surface charge due to the space charge is then

$$\rho_{sc} = eN_D^0 [1 - \exp(e\varphi_s/kT)] \quad (5.9)$$

When no space charge is present, the oxide can be treated as a dielectric and the surface charge is given by the equation

$$\rho_{sd} = -\epsilon\epsilon_0 \frac{V}{\delta} \quad (5.10)$$

where δ is the oxide thickness with opposite sign of x .

If space charge is present, the surface charge density will be the sum of the two charge densities, i.e.

$$\rho_s = eN_D^0 [1 - \exp(e\varphi_s/kT)] - \epsilon\epsilon_0 \frac{V}{\delta} \quad (5.11)$$

As Equation (5.2) shows, ρ_s plays an important role in determining the capacity of the electrode. Whether the Mott-Schottky approximation should be used or the oxide has to be treated as a dielectric is largely determined by Equation (5.11). If the first term is dominating, the Mott-Schottky approximation is likely to be valid. If the second term is dominating, the oxide will probably behave like a dielectric.

Based on Equation (5.11) the following inequality shows the range of φ_s where the dielectric properties are dominating

$$\ln(1 + \frac{\epsilon\epsilon_0}{eN_D^0} \frac{V}{\delta}) < e\varphi_s/kT < \ln(1 - \frac{\epsilon\epsilon_0}{eN_D^0} \frac{V}{\delta}) \quad (5.12)$$

In Figure 5.4 this range is shown vs the value of $-(\epsilon\epsilon_0/eN_D^0)(V/\delta)$. As can be seen, dielectric dominance is expected in the vicinity of $\varphi_s = 0$. The range broadens when the value of $-(\epsilon\epsilon_0/eN_D^0)(V/\delta)$ is increased. On both sides of the range, space charge should be dominating.

Since φ_s is likely to be very small when the electrode potential is in the vicinity of

the stabilization potential*, the dielectric properties should be dominating here. This is also found experimentally since the capacitance tends to be potential independent in this range, see Figure 5.3.

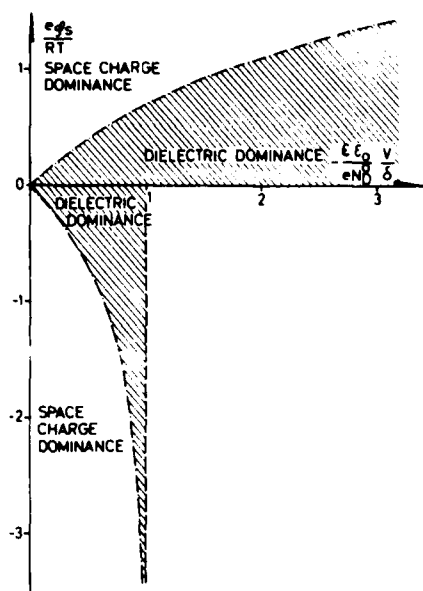


Figure 5.4 The range of ϕ_s which causes the surface charge to be dominated by the dielectric properties and by the space charge properties, respectively

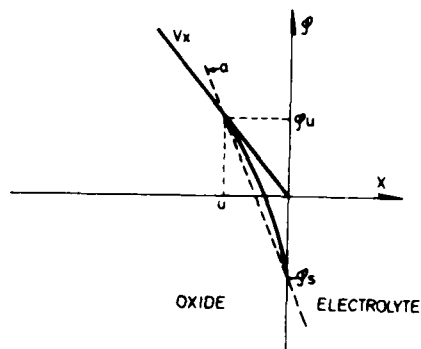


Figure 5.5 A schematic diagram of the potential distribution in the oxide near the surface

"a" indicates the approximate potential distribution in the space charge layer.

Equation (5.2) shows that in addition to the surface charge density ρ_s , there is another important parameter which determines the capacity. That is the integral

$$I_T = \int_{\phi_s}^{\phi_{\infty}} \rho d\phi = eN_D^0 \left[\int_{\phi_s}^{\phi_{\infty}} \exp(e\phi/kT) d\phi - \int_{\phi_s}^{\phi_{\infty}} \exp(e\phi/kT) d\phi \right] \quad (5.13)$$

As the equation shows, the integral can be divided into two parts

$$I_1 = \int_{\phi_s}^{\phi_{\infty}} \exp(e\phi/kT) d\phi \quad (5.14)$$

and

$$I_2 = \int_{\phi_s}^{\phi_{\infty}} \exp(e\phi/kT) d\phi \quad (5.15)$$

I_2 can easily be integrated, giving the following equation

$$I_2 = \frac{kT}{e} \left[\exp(e\phi_{\infty}/kT) - \exp(e\phi_s/kT) \right] \quad (5.16)$$

I_1 on the other hand is very difficult to resolve. It may, however, be worth while to divide it into two parts according to Figure 5.5.

* At the stabilization potential virtually no space charge layer should be present due to the straight electric field produced by the steady state ionic transport

In the first part, i.e. for $x = 0$ to $x = u$, the space charge layer is dominating. In the second part, i.e. for $x = u$ to $x = -\infty$, the electric field can be treated as nearly constant. In that case we have

$$I_1 = \int_{\varphi_s}^{\varphi_u} \exp(e\varphi/kT) d\varphi + \int_{\varphi_u}^{\varphi_\infty} \exp(e\varphi/kT) d\varphi \quad (5.17)$$

where the second part readily can be integrated since $\varphi = x \cdot V$ there. By introducing the result into Equation (5.13), the following equation for I_T is derived

$$I_T = eN_D^0 \left[\int_{\varphi_s}^{\varphi_u} \exp(e\varphi/kT) d\varphi - \frac{kT}{e} \exp(e\varphi_u/kT) + \frac{kT}{e} \exp(e\varphi_s/kT) \right] \quad (5.18)$$

The integral in Equation (5.18) is still difficult to resolve. An approximate solution can, however, be obtained if the potential in the space charge layer is assumed to follow a straight line, line "a" in Figure 5.5. In that case

$$\varphi - \varphi_s \approx \frac{x}{u} (\varphi_u - \varphi_s) \quad (5.19)$$

and

$$d\varphi \approx \frac{\varphi_u - \varphi_s}{u} dx \quad (5.20)$$

If this is introduced into Equation (5.18), the following solution can be obtained

$$I_T \approx N_D^0 kT \left[\exp(e\varphi_s/kT) - \frac{\varphi_s}{\varphi_u} \exp(e\varphi_u/kT) - \left(1 - \frac{\varphi_s}{\varphi_u}\right) \right] \quad (5.21)$$

which introduced into Equation (5.2) gives

$$\frac{\rho_s^2}{C^2} = V^2 + \frac{2}{e\epsilon_0} N_D^0 kT \left[\exp(e\varphi_s/kT) - \frac{\varphi_s}{\varphi_u} \exp(e\varphi_u/kT) - \left(1 - \frac{\varphi_s}{\varphi_u}\right) \right] \quad (5.22)$$

Three cases which may be of importance to the experiments may now be discussed:

- The space charge is of minor importance. In that case φ_s and φ_u are both in the vicinity of zero.
- φ_s has a large negative value due to anodic polarization. φ_u is still small due to either a small electric field inside the oxide or due to a space charge layer which is concentrated at the surface.
- φ_s has a large negative value and φ_u has a large value due to a space charge layer which extends into the oxide where also part of a straight electric field exists.

In case a $\exp(e\varphi_s/kT)$ and $\exp(e\varphi_u/kT)$ can be expressed in the form $1 + e\varphi_s/kT$ and $1 + e\varphi_u/kT$ respectively. This results in the second term in Equation (5.22) vanishing and the equation becomes equal to

$$\frac{\rho_s^2}{C^2} \approx V^2 \quad (5.23)$$

Since $\rho_s = -\epsilon\epsilon_0 \frac{V}{\delta}$ in that case, the equation for the parallel plate condenser is obtained, i.e.

$$C = \frac{\epsilon\epsilon_0}{\delta} \quad (5.1)$$

This clearly shows that thickness measurements can be made by using the capacity if the electrode potential is in the vicinity of the stabilization potential where φ_s and φ_u are small.

In case *b* $\exp(e\varphi_u/kT)$ can still be expanded while $\exp(e\varphi_s/kT)$ goes towards zero. Equation (5.22) will then be

$$\frac{\rho_s^2}{C^2} = V^2 - \frac{2}{\epsilon\epsilon_0} N_D^0 e\varphi_s - \frac{2}{\epsilon\epsilon_0} N_D^0 kT \quad (5.24)$$

Since now $\rho_s \approx eN_D^0$, the inverse square of the capacity will be

$$\frac{1}{C^2} \approx \frac{V^2}{e^2 N_D^{02}} - \frac{2}{\epsilon\epsilon_0} \frac{kT}{e^2 N_D^0} - \frac{2}{\epsilon\epsilon_0} \frac{\varphi_s}{N_D^0} \quad (5.25)$$

which is a modified Mott-Schottky equation. The slope of the line in the Mott-Schottky plot will have the usual value except for N_D^0 being now the donor concentration in the oxide surface towards the electrolyte and not necessarily that of the bulk oxide.

In case *c* Equation (5.22) will be

$$\frac{\rho_s^2}{C^2} \approx V^2 - \frac{2}{\epsilon\epsilon_0} N_D^0 kT \exp(e\varphi_u/kT) \cdot \frac{\varphi_s}{\varphi_u} \quad (5.26)$$

Since $\rho_s \approx eN_D^0$ still is to be expected, the inverse square of the capacity will be

$$\frac{1}{C^2} = \frac{V^2}{e^2 N_D^{02}} - \frac{2}{\epsilon\epsilon_0} \frac{kT}{eN_D^0} \exp(e\varphi_u/kT) \frac{\varphi_s}{\varphi_u} \quad (5.27)$$

which shows that a straight line in a Mott-Schottky plot is still to be expected, but with a slope which is $\frac{1}{e\varphi_u} \exp(e\varphi_u/kT)$ greater than the normal slope. Since $\varphi_u \gg kT/e$, $\frac{1}{e\varphi_u} \exp(e\varphi_u/kT) > 1$, which indicates a steeper curve.

If cases *a* and *c* are compared with the experimental results, case *b* seems to be more likely than case *c*. By using *c* an even higher donor concentration than those given will be obtained. This is very unlikely since the donor concentration is already extremely high. For such donor concentrations the Debye length will be very short, indicating that most of the space charge layer will be situated just beneath the oxide surface. This is also in accordance with the assumptions made in case *b*. This gives a strong indication that the donor concentrations obtained from the experiments when the Mott-Schottky approximation is used, really represent those existing in the oxide surface.

A similar conclusion was also drawn by Schultze *et al* (15) when treating the oxide film on iron. They pointed out, however, that with such high donor concentrations the dielectric constant must be much higher than in normal oxides. If this is assumed also for Al, the calculated donor concentrations have to be reduced by approximately one order of magnitude.

6 THE INFLUENCE OF IMPURITIES ON ALUMINIUM

6.1 General

In a review article concerning impurity effects on the corrosion of aluminium, Franke (21) in 1955 stated that the protective properties of the surface film on this metal are extraordinarily strongly affected by impurities. The effect is usually a negative one, *i.e.*, while the pure metal is relatively corrosion resistant, the addition of impurities largely decreases the resistivity.

The impurities can act in two ways:

- a) They may form local elements in the surface, which may act as local cells
- b) They may enter the oxide film evenly and change the properties of the film

Early and also more recent works on impurity effects emphasize the local effect. Franke, for instance, stresses that when the impurities are in solid solution, their influence is relatively insignificant (21).

Straumanis *et al* (71) studied the effect of minor alloying elements on the corrosion of Al. The test samples were immersed into 0.5 N solutions of NaOH, Ba(OH)₂ and NH₄OH and kept at open circuit. On the basis of weight loss measurements they found that when elements like Pt, Fe and Cu, which normally have low hydrogen overvoltage, were alloyed into Al, the corrosion rate increased. The increase was proportional to the logarithm of the concentration of these elements in the alloy.

With elements like Zn, Sn, Pb and Si, the corrosion rate either increased slightly, was retarded, or there was no effect on the corrosion rate at all.

Straumanis *et al* concluded that "... the fact that the rate of dissolution of Al in basis increases gradually with the content of minor metals of low overpotential can be explained only by the activity of local elements".

Since the corrosion rate is dependent on the rates of both the anodic Al dissolution reaction and the cathodic reaction (either the hydrogen evolution or the oxygen reduction), the effect of the impurities will be difficult to analyse from the above results. The anodic and cathodic reactions have to be separated.

Kunze (47) performed electrochemical studies on aluminium containing $4 \cdot 10^{-2}\%$ Fe, and compared the results with those obtained with pure Al. The Fe content was either homogeneously dispersed in the Al or formed separate eutectic phases, *i.e.* Al₃Fe. In both cases the cathodic reaction, *i.e.* the hydrogen evolution, was influenced by the Fe content. No data were presented on the effect of Fe on the Al-dissolution reaction.

Kunze interprets his data by assuming that local cathodic sites are formed. Even in the case of homogeneously dispersed Fe he assumes that Al dissolves, leaving Fe behind in the surface, which then acts as cathodic sites.

Although not studying the impurity effects in particular, Nisancioglu *et al* (56) observed that highly localized attack took place on their relatively impure Al-electrode when it was cathodically polarized. Since the effect was especially observed in unbuffered solutions, they assumed that the attack was caused by a local increase in the alkalinity due to higher hydrogen evolution in the vicinity of the impurities. The enhanced hydrogen evolution was explained as due to either a formation of local cathodic sites or as an increase in the electronic conductivity of the barrier layer here.

That such an increase in electronic conductivity is to be expected was demonstrated as early as in 1936 by Hartmann (29). During a study of the electric conductivity of Al_2O_3 he found that the conductivity at room temperature increased 1000 times, *i.e.* from $\sim 10^{-7} \Omega^{-1} \text{m}^{-1}$ to $10^{-4} \Omega^{-1} \text{m}^{-1}$, when small amounts of Fe were introduced.

In order to study the influence of such effects on the electrochemical properties, it is desirable to have an alloy where all the impurities are dissolved in the Al metal. Certainly the effects may still be there when local phases are present. It is, however, likely that the oxide above and in the vicinity of these phases will behave differently than the rest. This will cause local effects which may be confused with the local cathodic effects described above.

There is one method of alloying which lends itself to studies of evenly distributed alloying elements; that is, ion implantation. When ions are sputtered onto a metal surface, they penetrate the surface and form an alloy beneath the surface. The ions behave here as if fully dissolved. Using this method, even metals which are normally completely insoluble in Al can be studied in the dissolved state. Ion implantation has been used by several authors in the study of impurity effects on Al (3-5,8,74).

Al-Saffar *et al* (5) showed that when Mo was implanted in thin Al foils, no sign of separate Mo phases could be seen by transmission electron microscopy after the implantation, indicating that Mo was fully dissolved. When the foils were aged at 393 K for 48 hours, separate phases of Mo were formed and could easily be seen under the electron microscope.

Using a three-sweep potentiodynamic polarization technique, Al-Saffar *et al* separated the anodic and cathodic reactions. They obtained a cathodic curve that was displaced approximately 0.4 V towards more noble potentials by the implantation. To test whether the implantation technique as such was responsible for the displacement, or whether it was due to Mo, Al and Ar ions were implanted. Except for the first scan, no effect was observed from Al and Ar ions. The results clearly show that Mo dissolved into Al decreases the cathodic polarization, *i.e.* enhances the hydrogen evolution. Since this also brings the open circuit potential in a noble direction, the oxide film will grow thicker. This again will probably give the Al-surface a more stable oxide film.

A similar effect was also found when Cr was implanted instead of Mo. Ni, on the other hand, behaved in quite a different manner. The Ni-alloyed electrode showed an even higher rate of hydrogen evolution than the Mo- and Cr-alloyed electrodes. The anodic reaction, which in the case of Mo and Cr underwent only small changes, was changed completely when Ni was implanted. When the anodic curve was compared with that of pure Ni, they were found to be nearly identical in the passive range. This indicates that the oxide film formed on Ni-implanted Al is converted to a film similar to that formed on passive Ni. This is in contrast to the effect of implanted Mo and Cr which merely modified the existing aluminium oxide film. The modification is probably a result of an increased electronic conductivity of the film since the hydrogen evolution reaction is enhanced.

When the common alloying technique *i.e.* melting is applied, one is restricted to using alloying elements which have a high degree of solubility in solid Al. Such an element is Si, which at 577°C has a maximum solubility of 1.59 At % (27). If therefore the alloy is quenched at this temperature, the Si should be evenly distributed. Since Si^{4+} is the most stable ion of Si, that ion will probably enter the oxide film where it will modify the electronic conduction of the film. Studies of such an alloy can thus reveal the action of dissolved impurities on the oxide film. If the results are compared with those obtained from alloys containing locally formed phases, a more detailed picture of the impurity effects can be obtained.

6.2 Experimental

The test electrodes consisted of super pure Al alloyed with certain amounts of alloying elements (Si, Fe and Sn).

Before use, the electrodes were abraded to 600 mesh with emery paper, etched in a lukewarm 10% NaOH solution, dipped into a 1% acetic acid solution and thereafter rinsed in distilled water.

The electrolyte consisted of an acetic acid sodium acetate buffer of pH = 5.25. The acetate concentration was kept constant at 1 M.

Before the experiments started, the test electrodes were kept overnight in the electrolyte at a certain potential, *i.e.* the stabilization potential. The temperature was $25 \pm 1^\circ\text{C}$. N_2 was bubbled through the electrolyte in order to remove O_2 .

In order to obtain the anodic and cathodic reaction rates *vs* the potential, the potential step technique described in Chapter 4 was used.

The Mott-Schottky plots used for calculating the donor concentrations were obtained by the same technique as that used in Chapter 5.

6.3 Results

Figure 6.1 shows typical Tafel plots obtained by the potential step method. The curves represent electrodes containing different amounts of Si (mole fractions from $2.4 \cdot 10^{-4}$ to $6.9 \cdot 10^{-3}$). The stabilization potential is the same, *i.e.* -1.1 V (SCE) . As can be seen, the cathodic curve is displaced towards higher *cd* values when the Si content is increased. The anodic curve is, on the other hand, hardly affected by the Si content.

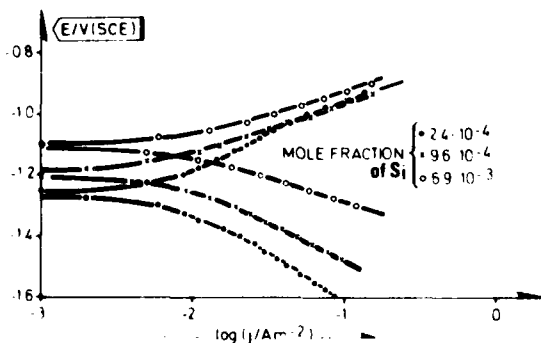


Figure 6.1 Anodic and cathodic Tafel curves from potential steps applied on Si containing Al-electrodes stabilized at -1.1 V (SCE) pH = 5.25

In Figure 6.2 the potential at a certain anodic *cd* is plotted *vs* the stabilization potential. The electrodes contain different alloying elements in different quantities. The straight line shown in the figure is identical to the central line shown in Figure 4.11 and represents the results obtained from unalloyed Al. As can be seen, the results from alloyed electrodes are scattered around the line. While the Si alloyed electrodes seem to lie nearly on the line, there seems to be a slight tendency for the Fe alloyed electrodes to be displaced somewhat towards higher stabilization potentials. The Sn

alloyed electrodes, on the other hand, seem to be displaced towards lower stabilization potentials. The displacements are, however, in both cases very small and may not be significant at all. The conclusion must therefore be that the alloying elements do not affect the anodic reaction rate to any great extent.

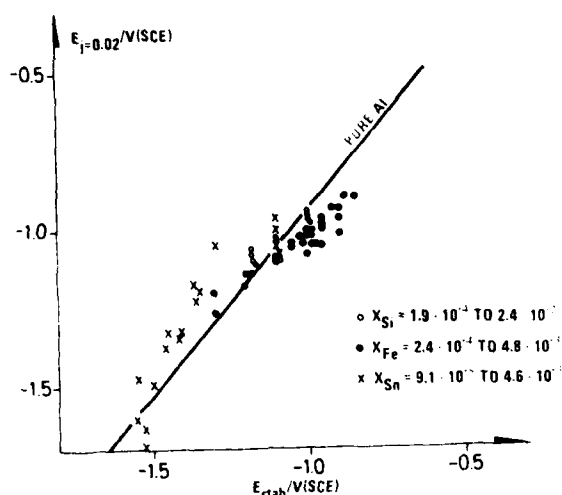


Figure 6.2 The electrode potential of different alloys at $j_a = 0.02 \text{ Am}^{-2}$ vs the stabilization potential $\text{pH} = 5.25$.

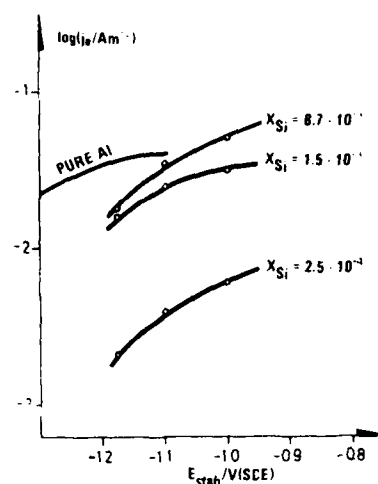


Figure 6.3 The cathodic reaction rate at a certain electrode potential (-1.25 V (SCE)) vs the stabilization potential

Mole fraction of Si is given by numbers in the figure.

In Figure 6.3 the cathodic reaction rate of Si alloyed electrodes is plotted vs the stabilization potential, *i.e.* vs the oxide thickness. The reaction rate chosen is that obtained at an electrode potential of -1.25 V (SCE) . The conditions correspond to those for the lower curve in Figure 4.13, but then for pure Al. Just as for pure Al, the cathodic reaction rate decreases with decreasing stabilization potential. The decrease is even larger for alloyed than for pure Al. If the reaction rates at a lower electrode potential are plotted instead, flatter curves are obtained, just as for pure Al. No straight line similar to the upper curve in Figure 4.13 was, however, seen.

As Figure 6.3 shows, the Si content in Al has a marked influence on the cathodic reaction rate. When the rate at a certain stabilization potential, *i.e.* a certain oxide thickness, is plotted vs the Si content in a log-log plot, a straight line with 45° slope is obtained at low Si concentrations, see Figure 6.4. This indicates a proportionality between the cathodic reaction rate and the Si content of the Al. When the mole fraction of Si is above $2 \cdot 10^{-3}$, the cathodic reaction rate becomes independent of the Si concentration. One remarkable fact is that the cathodic reaction rate for pure Al is always above the rates obtained with the Si alloyed Al.

The results from the capacity measurements are shown in Figure 6.5 as Mott-Schottky plots. The figure shows that, like pure Al, the capacity for alloyed electrodes is potential dependent. From the slope of the straight lines it can be seen that the electrode containing the smallest amount of Si also has the lowest donor concentration, *i.e.* the highest slope. The more Si the electrode contains, the lower becomes the slope, indicating a higher donor concentration. This implies that Si ions enter the

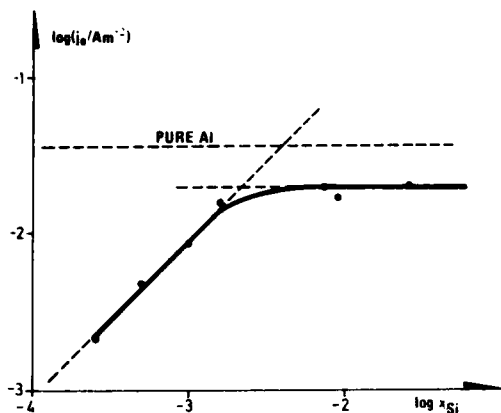


Figure 6.4 The logarithm of the cathodic reaction rate at -1.25 V (SCE) vs the logarithm of the Si mole fraction
 $E_{\text{stab}} = -1.175$ V (SCE).

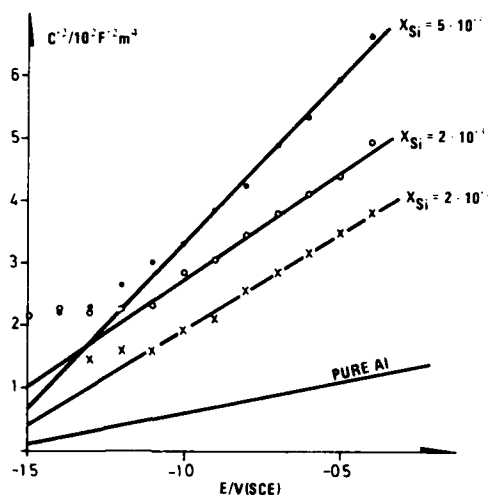


Figure 6.5 Mott-Schottky plots of Si containing Al-electrodes stabilized at -1.1 V (SCE).

oxide from the alloy and act as donors in the oxide. But, once more, the pure Al behaves in a peculiar way and has a higher donor concentration than the Si alloyed electrodes.

Also iron influences the cathodic reaction rate. In Figure 6.6 this rate at a certain electrode potential is plotted vs the stabilization potential. The plot is similar to that in Figure 6.3, but now the alloying element is Fe.

As can be seen from the figure, the Fe-alloyed electrodes differ from those alloyed with Si in that they have higher reaction rates than the pure Al electrode. An exception is the electrode having the smallest concentration of Fe, *ie* with a mole fraction of $1.26 \cdot 10^{-4}$.

There seems to be a general increase in the cathodic reaction rate with increasing stabilization potentials. The data on the right-hand side of the figure, which represent high stabilization potentials, are, however, quite irreproducible. The exact shape of the curves is therefore difficult to establish. On the left-hand side the data are more reproducible. These data are therefore used to determine the relationship between the reaction rate and the concentration of Fe in Al, see Figure 6.7. By comparing this figure with Figure 6.4, it can be seen that the Fe-alloyed electrodes differ from Si-alloyed electrodes in various ways. Generally the Fe addition has a greater effect on the reaction rate than the corresponding Si addition. No maximum reaction rate is observed and the curve deviates from a straight line at low concentrations. But just as for Si, a small addition of Fe to pure Al seems to reduce the reaction rate. To obtain this latter effect, the Fe additions must, however, be extremely small.

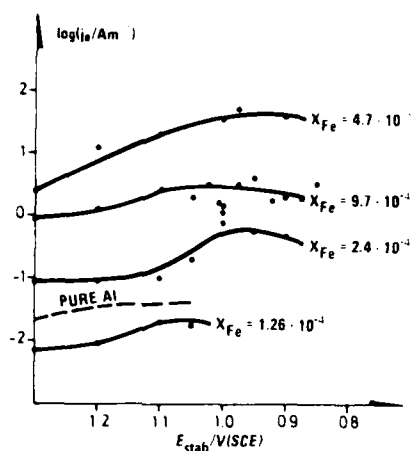


Figure 6.6 The cathodic reaction rate at an electrode potential of -1.25 V (SCE) vs the stabilization potential

Mole fraction of Fe is given by numbers in the figure.

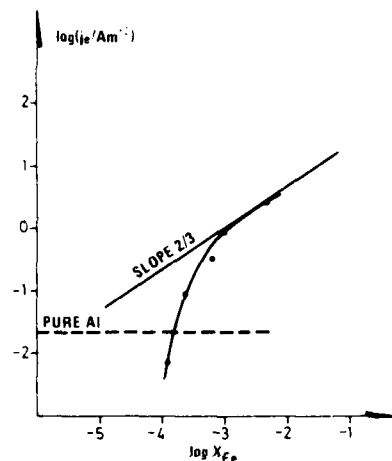


Figure 6.7 The logarithm of the cathodic reaction rate at -1.25 V (SCE) vs the logarithm of the Fe mole fraction

6.4 Discussion

The fact that the anodic reaction is nearly independent of the impurities has several implications.

First of all, it shows that the ion transport through the oxide film is still dominant in the metal oxidation process. Weak areas in the vicinity of an impurity concentration may give rise to local effects which can be seen under the microscope. Such effects can, however, hardly play an important role. At most, they may cause a slight deviation from the line in Figure 6.2.

Since the alloyed electrodes roughly follow the straight line in the figure, it can be assumed that the same relationship between the stabilization potential and the oxide thickness described in Chapter 4 for pure Al, also is valid for alloyed Al. This may be an important fact to be aware of when the cathodic reaction rate is considered.

Unlike the anodic reaction, the cathodic reaction depends strongly on the alloying elements. As shown in Figure 6.4, the cathodic reaction rate is linearly dependent on the Si concentration up to a certain limit.

In Chapter 4 it was suggested that the cathodic reaction could be used as a measure of the electronic conductivity and thereby be a measure of the free electron concentration in the oxide. Since Si alloyed into the metal increases the free electron concentration of the oxide, Si probably enters the oxide from the metal and acts as a donor in the oxide film.

When the mole fraction of Si in the alloy is increased beyond $\sim 2 \cdot 10^{-3}$, no further increase in reaction rate is observed. This indicates that the oxide at this concentration is saturated with Si.

That Si really acts as a donor can be seen from Figure 6.5 which shows Mott-Schottky plots for Si-alloyed electrodes. Since the slope of the lines in such plots is

inversely proportional to the donor concentration, the figure shows that the donor concentration increases with increasing Si content in the alloy. As further shown by the figure, the difference in donor concentration between the two electrodes containing the highest amounts of Si is very small. This is also to be expected since they are both in the saturation range shown in Figure 6.4.

A calculation of the donor concentration in the oxide on the alloy containing an Si mole fraction equal to $2 \cdot 10^{-2}$ shows that $3.8 \cdot 10^{26}$ donors are present per cubic meter, provided that the relative dielectric constant of the oxide is 12. If the specific gravity of the oxide is 3.423 g/cm^3 (25), the oxide will contain $1.01 \cdot 10^{29}$ ions per cubic meter. Assuming the donors to be identical to the Si ions, the mole fraction of Si ions in the oxide will be $3.7 \cdot 10^{-3}$. Schultze *et al* (67) points out that oxides having such high donor concentrations probably will have dielectric constants at least ten times larger than the normal oxide. In that case the donor concentration, and thereby the mole fraction of Si in the oxide, must be reduced correspondingly. The maximum solubility of Si in the oxide must then be in the order of $3.7 \cdot 10^{-4}$ to $3.7 \cdot 10^{-3}$, depending on the dielectric constant.

The equilibrium constant for the distribution of Si between the oxide and the metal,

$$x_{\text{Si}}(\text{ox})/x_{\text{Si}}(\text{al}) = k_{\text{Si}} \quad (6.1)$$

can also be calculated. This can be done by using the maximum donor concentration and the alloy concentration where the sloped line in Figure 6.4 intersects the horizontal line. The calculation shows that k_{Si} has a value between 0.16 and 1.6 depending on the dielectric constant.

Despite the fact that the free electron concentration increases with increasing Si content in the alloy, both Figures 6.4 and 6.5 show that pure Al contains more free electrons than the Si alloyed Al. This can be explained either by assuming that small amounts of Si form trapping centres for electrons in the oxide or that the oxide on pure Al contains a larger number of stoichiometric defects than the oxide on the Si-alloyed Al. As pointed out by Heusler *et al* (35) for niobium oxide and by Möller *et al* (53) for tin oxide, stoichiometric defects may act as donors. In that case the primary action of small Si additions is to decrease these defects and then, if more Si is added, to act as donors themselves.

In Figure 6.5 the electrode having the smallest amount of Si ($x_{\text{Si}} = 5 \cdot 10^{-5}$) has a lower slope than might be expected. An extrapolation of the sloped line in Figure 6.4 to an Si concentration equal to $5 \cdot 10^{-5}$ gives an extremely low donor concentration. Since such a low donor concentration is not found in the Mott-Schottky plot, see Figure 6.5, the extrapolation is probably not valid. The explanation for the discrepancy may be that the donors which exist in the oxide on pure Al are not fully neutralized by such a small Si addition. The actual donor concentration is therefore higher than would be expected from the extrapolation of data obtained with electrodes of higher Si content.

With a constant Si content the cathodic reaction rate is seen to increase with increasing stabilization potential. This was also found with pure Al at relatively high potentials, see the lower curve in Figure 4.13. The increase is more marked on the Si alloyed electrodes, however, especially when the Si content is low. The increase may not have anything to do with the oxide thickness, but may merely be an effect of the space charge layer in the oxide surface towards the electrolyte. The increased reaction rate indicates that the electron concentration in the oxide surface towards the electrolyte is increased on an increase in the stabilization potential. That such an increased electron concentration is likely to occur can be illustrated by the potential distribution scheme used by Vetter (83) but modified to include space charge layers. Such a modified scheme is shown in Figure 6.8. In this figure the potential distribution is

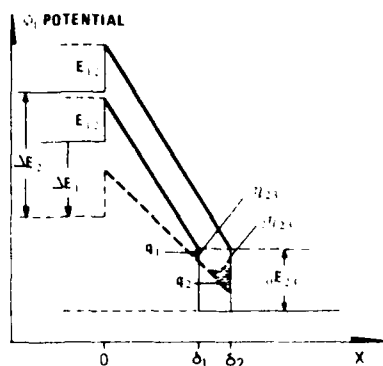


Figure 6.8 The potential distribution in the electrode during potential transient experiments when space charge is present

electrons in the surface than a step made to the same potential but from a lower potential. Obviously, this effect is more pronounced on oxides having a low concentration of free electrons than on oxides where the concentration is high. Since electrodes containing small amounts of Si also have the lowest electron concentration, the effect should be more pronounced on such electrodes. This seems also to be the case, see Figure 6.3.

Unlike Si, Fe has a low solubility in Al. The mole fraction at maximum solubility (at 655°C) is as low as $2.52 \cdot 10^{-4}$ (6). Above this concentration FeAl_3 is formed. At 600°C, where the alloys used are homogenized, the mol fraction of soluble Fe is $1.2 \cdot 10^{-4}$. This means that among the alloys tested, only that having the lowest mole fraction of Fe, i.e. $1.26 \cdot 10^{-4}$, will have Fe mainly in the dissolved state. All the other alloys will contain Fe mainly in the FeAl_3 phase.

When the two phases are in equilibrium, the activity of Fe dissolved in Al is given by the equilibrium conditions. This means that when the Al is saturated with Fe, the activity of Fe dissolved in Al will be constant and independent of the excess Fe. In our case a certain Fe activity is obtained at 600°C. When the alloy is quenched, Al will be supersaturated with Fe. If no FeAl_3 is formed during the quenching process, the activity of Fe will be that existing at 600°C but corrected for the change in temperature. In spite of this change, the activity should still be independent of the Fe excess. It will, however, be very sensitive to the homogenization temperature. If only the dissolved Fe were involved in the cathodic process, the cathodic reaction rate would be independent of the total amount of Fe. As Figures 6.6 and 6.7 show, this is not the case. The reaction rate is highly dependent on the total Fe content. This gives a strong indication that the observed increase in reaction rate is due to the FeAl_3 phase.

Since the FeAl_3 phase is randomly distributed on the surface, an uneven action on the oxide film is to be expected. The change in electronic properties will probably be larger immediately above and in the vicinity of the FeAl_3 phase. Local effects are therefore to be expected. Since the fraction of the surface occupied by the FeAl_3 phase is roughly proportional to the $2/3$ power of the total amount of Fe in the alloy, the experimental data should follow the line with slope equal to $2/3$ indicated in Figure 6.7.

shown for two electrodes stabilized at two different potentials. From these potentials, steps are made to one and the same electrode potential (the broken curve in the figure). The magnitude of the steps are denoted ΔE_1 and ΔE_2 respectively. The largest part of the change is assumed to take place across the oxide. In that case the changes at the oxide electrolyte interface, i.e. ${}_1\eta_{2,3}$ and ${}_2\eta_{2,3}$ in the figure, become small. The result is an upward bending of the potential curve in the oxide near the surface like that indicated in the figure. The electrode which is stabilized at the highest potential, i.e. in the figure has an oxide thickness equal to δ_2 , will have the largest bending and thereby also the most negative space charge layer. The surface electron concentration will therefore also be high on this electrode. In general, it is therefore to be expected that a step made from a high potential will create more

The distribution of FeAl_3 may vary from electrode to electrode and even from surface to surface. Some irreproducibility is therefore to be expected. This may explain why highly irreproducible results are observed in Figure 6.6, especially at higher stabilization potentials.

At low Fe concentrations the cathodic reaction rate decreases quite rapidly with decreasing concentrations of Fe. The rate becomes even smaller than the rate for pure Al, see the results from the electrode having the lowest Fe concentration. This is in accordance with the results obtained on Si alloyed electrodes. Since the Fe concentration then is in the vicinity of that corresponding to maximum solubility, Fe will mainly be dissolved here. This may explain why similar effects as those observed on Si-alloyed electrodes are observed at low Fe concentrations. In low concentrations, also Fe seems to decrease the donor concentrations caused by the stoichiometric defects in the oxide.

When Fe is used as alloying element, no saturation effects like those observed on Si are found. In the total range studied, the cathodic rate increases with an increase in the Fe content. This indicates that the solubility of Fe in the oxide is higher than that of Si. This is also reasonable, since $\gamma'\text{Fe}_2\text{O}_3$ and $\gamma'\text{Al}_2\text{O}_3$ are very similar. The oxide above and in the vicinity of FeAl_3 may therefore contain a high concentration of Fe which may give rise to the high electronic conductivity indicated by the high cathodic reaction rate. The experimental results are in this context quite meagre, however. No safe conclusions can therefore be drawn.

The experiments have shown that no serious effects of alloying elements are found on the anodic metal dissolution reaction. The cathodic reaction is, on the other hand, highly influenced by the alloying elements. Both the elements dissolved in the Al phase and those forming separate phases seem to be active. They seem to enter the oxide and have there two effects. In low concentrations they reduce the donors in the oxide formed by stoichiometric defects. In higher concentrations they act as donors themselves.

7 THE PROPERTIES OF OXIDE COVERED Al – AN OVERVIEW

The electrochemical properties of aluminium in aqueous solutions depend totally on the properties of the oxide film which is formed on the metal surface. The film, and thereby the metal, is quite stable in neutral solutions. In acid and alkaline solutions the metal dissolves readily, but even this dissolution takes place via the oxide film (34).

Two main groups of oxides are formed on the metal surface during anodization: the barrier film and the porous film. Which of these is the dominating film depends on the electrolyte where the anodization takes place. The barrier film is probably always formed to some extent. In some electrolytes it is the only film. It may grow to approximately 5000 Å when sufficient anodization voltage is present. The steady state anodic film will then be proportional to the anodizing voltage.

In some electrolytes the barrier film can grow only to a certain thickness. If a constant anodic current is flowing, the potential will first increase to a certain value. When this is reached, the voltage will flatten and may even drop somewhat before it becomes constant. The film will, however, continue to grow beyond this point. Upon the barrier film which was first formed, a new porous oxide film will be built up. The porous layer may become relatively thick.

The barrier layer is very compact and consists mainly of γ' -Al₂O₃, which has a highly disordered inverse spinel structure (80). A similar structure, γ -Fe₂O₃, is also found on passive iron (92). It is usually assumed that it is the barrier oxide which determines most of the electrochemical properties of the oxide covered Al-electrode (7), since both ion and electron transport is hampered, but has to take place through this oxide. In steady state a nearly constant electric field in the order of $7 \cdot 10^8$ V/m exists across the barrier film (88). This field is due to a constant ion transport through the film which is necessary for fulfilling the conditions at the barrier oxide-electrolyte interface in steady state. These conditions are set by the oxygen exchange reaction between the barrier oxide and the electrolyte, which in steady state has to proceed at equilibrium.

Even though most of the electric field is situated across the barrier layer and the transport processes therefore are mainly controlled by this film, the porous layer may play a certain role (57). This is mainly due to the electrolyte diffusion barrier which the porous film represents. Concentration differences inside the porous oxide may then easily occur. Such effects will especially be observed in unbuffered solutions and when the cathodic hydrogen evolution reaction is enhanced. In that case a rise in pH at the barrier oxide surface will take place. Such an enhanced hydrogen evolution may be observed on impure Al and also when the potential is lowered. The change in pH may give rise to the enhanced attack of the aluminium electrode observed at low potentials in connection with "cathodic corrosion" (57).

Thermodynamic calculations may give the electrode potential where no electric field exists across the oxide (69). Although it is pH dependent, this potential is usually far below potentials normally obtained on the Al-electrode, which means that an "anodic" field is nearly always present across the oxide. The experiments described in this work indicate that also when no outer "anodization" voltage is applied to the electrode, the field across the oxide film in steady state is nearly constant. Consequently, the proportionality between the potential difference across the oxide in steady state and the oxide thickness is still the same as that found during anodization. Even if the cathodic reaction is dominating and a cathodic total current is flowing, the proportionality seems to exist. This means that the potential at which the electrode is stabilized, *i.e.* the stabilization potential, plays an important role in determining the

oxide thickness. When the stabilization potential is low, extremely thin oxides may be present on the electrode surface.

Except for very low stabilization potentials, the steady state anodic reaction rate seems to be nearly independent of the potential. This is however probably only the case in buffered solutions where the pH is kept constant at the electrode surface. The same rate can then be found whether the electrode potential is 5 V (SCE) or -0.9 V (SCE). This indicates that the relationship found during anodization between the steady state anodic rate and the field across the film is still valid at low potentials. This can also be shown by measuring the change in current density during potential steps. If the steps are of short duration, the electric field across the oxide can be changed without changing the oxide thickness. The relationship between the field strength and the anodic reaction rate is then found to be the same as that observed during anodization.

When an electrode is anodized to a certain voltage and a barrier oxide with a certain thickness is formed, the oxide can be thinned down again by decreasing the voltage. The thinning process is, however, very slow and several days may elapse before a new steady state thickness is arrived at. This is demonstrated by capacity measurements. A slow thinning is also to be expected since the film dissolution rate is determined by the slow process of oxygen ions being transferred from sites in the oxide to an adsorbed state, a process which is only weakly dependent on the potential. The growth of the film is, on the other hand, determined by the opposite reaction, and since the concentration of adsorbed oxygen ions is highly potential dependent, the rate of growth can be greatly increased by an increase in the anodic potential (91).

Capacity measurements show that two types of capacities are observed: one which is independent of potential steps and one which decreases with increasingly positive potential steps.

The potential independent capacity can be treated as a parallel plate condenser and gives us a means of determining the oxide thickness. The thickness-potential relationship could be verified by this method.

The potential dependent capacity could be treated according to the Mott-Schottky approximation whereby the donor concentration in the oxide could be determined. In accordance with the results from iron electrodes covered with thin oxide films (70), extremely high donor concentrations were also found on Al-electrodes, indicating a highly disordered oxide. The donor concentration could be decreased by adding small alloying elements to the Al-metal, indicating that these elements enter the oxide where they are able to decrease the defects in the structure to some extent.

The alloying elements seem to have insignificant effects on the anodic metal dissolution. The ion transport through the oxide, and thereby also the thickness-voltage relationship, seems therefore not to be affected by these elements.

The cathodic hydrogen evolution reaction, on the other hand, is highly affected. Small amounts of alloying elements seem to decrease the cathodic reaction rate just as they decrease the donor concentration. This indicates that the cathodic hydrogen evolution reaction rate is determined by the electronic properties of the oxide.

When small amounts of Si are alloyed into Al, they dissolve completely in the metal. Experiments with such alloys have shown that the cathodic reaction rate at a certain potential is proportional to the Si mole fraction up to a certain limit where it is independent of further Si additions. This limit is below the solubility limit of Si in Al. It is believed that the oxide at this point is saturated with Si. Even though the

cathodic reaction rate increased with increasing Si content, it remained below the rate observed on super pure Al, indicating that the donors formed by the Si addition are still less than those formed by stoichiometric defects in the oxide on pure Al.

When Fe is alloyed into Al, a separate phase, Al_3Fe , is formed and only an extremely low amount of Fe is dissolved in the Al phase. This indicates that the Al will be saturated with Fe even when the Fe addition is small. In spite of this, the cathodic reaction rate is increased by the Fe additions and no limiting rate like that of Si is observed. The rate soon becomes much faster than on pure Al. This gives a strong indication that not only impurity elements dissolved in the metal, but also those able to form separate phases may influence the cathodic reaction rate. It is to be expected that in the latter case the oxide will be unevenly affected and local effects will arise. Even though the anodic reaction *a priori* is not affected, a slight enhancement in the vicinity of the local phases is to be expected, either due to a weaker oxide here or due to higher alkalinity. The latter will probably be more pronounced in unbuffered solutions. Such local effects have been observed by several authors.

As the oxide properties play an important role for the stability of the metal, the effect of the impurities gives us a means of controlling these properties and thereby the stability of the metal. By introducing the right impurities in the right manner, it should be possible to compose oxide films which have properties best suited for a certain utilization.

On the other hand, the oxide properties are very sensitive to changes in the surrounding medium. The stability of the metal will therefore be vulnerable to minor constituents which are difficult to control.

References

- (1) Allard K D, Ahrens M, Heusler K E (1975): *Werkstoffe unter Korrosion* 26, 694.
- (2) Allard K D, Heusler K E (1977): *J Electroanal Chem* 77, 35.
- (3) Al-Saffar A H, Ashworth V, Grant W A, Procter R P M (1977): Proc 6th European Congress on Metallic Corrosion SCI, London, 13.
- (4) Al-Saffar A H, Ashworth V, Grant W A, Procter R P M (1978): *Corros Sci* 18, 687.
- (5) Al-Saffar A H, Ashworth V, Bairamov A K O, Chivers D J, Grant W A, Procter R P M (1980): *Corros Sci* 20, 127.
- (6) Altenpohl D (1965): *Aluminium und Aluminiumlegierungen*, Springer-Verlag, Berlin.
- (7) Anderson P G, Devereux O F (1975): *J Electrochem Soc* 122, 267.
- (8) Brown F, Mackintosh W D (1973): *J Electrochem Soc* 120, 1096.
- (9) De Gryse R, Gomes W P, Cardon F, Vernik J (1975): *J Electrochem Soc* 122, 711.
- (10) De Smet D J (1976): *Electrochim Acta* 21, 1137.
- (11) Dewald J F (1960): *Bell Syst Techn J* 39, 615.
- (12) de Wit H J, Wijenberg C, Crevecoeur C (1979): *J Electrochem Soc* 126, 779.
- (13) DiBari G A, Read H J (1971): *Corrosion* 27, 483.
- (14) Diggle J W, Downie T C, Goulding C W (1969): *Chem Rev* 69, 365.
- (15) Dignam M J, Ryan P J (1968): *Can J Chem* 46, 549.
- (16) Dogonadze R R, Kuznetsov A M, Ulstrup J (1977): *Electrochim Acta* 22, 967.
- (17) Drazic D M, Despic A R, Zecevic S, Atanackovic M (1979): *Power Sources 7* (Ed D H Collins), Academic Press, London, New York.
- (18) El-Basiouny M S, Haruyama S (1977): *Corros Sci* 17, 405.
- (19) Fateev Y F, Vrzhosek G G, Antropov L I (1973): *Tr Ukr Respub Konf, Elektrokhim* 1, 189.
- (20) Franck V F, Weil K G (1952): *Z Elektrochem Ber Bunsenges physik Chem* 56, 814.
- (21) Franke E (1953): *Werkstoffe und Korrosion* 4, 4.
- (22) Geana D, El-Miligy A A, Lorenz W J (1974): *Corros Sci* 14, 657.
- (23) Gerisher H, Vielstich W (1955): *Z physik Chem NF* 3, 16.

- (24) Gerischer H (1961): Advances in electrochemistry and electrochemical engineering, *Interscience, New York* 1, 154.
- (25) Gorn F (1975): *Z physik Chem NF* 98, 233.
- (26) Gunterschultze A, Betz H (1934): *Anal Physik* 92, 367.
- (27) Hansen M (1958): Constitution of Binary Alloys, McGraw-Hill Book Company, New York.
- (28) Harkness A C, Young L (1966): *Can J Chem* 44, 641.
- (29) Hartmann W (1936): *Z Physik* 102, 709.
- (30) Hass G (1949): *J Amer Opt Soc* 39, 532.
- (31) Heusler K E (1968): *Z Elektrochem Ber Bunsenges physik Chem* 72, 1179.
- (32) Heusler K E (1975): *Electrochim Acta* 20, 237.
- (33) Heusler K E (1978): *Ber Bunsenges physik Chem* 82, 297.
- (34) Heusler K E, Allgaier W (1971): *Werkstoffe u Korrosion* 22, 297.
- (35) Heusler K E, Schulze M (1975): *Electrochim Acta* 20, 237.
- (36) Heusler K E, Yun K S (1977): *Electrochim Acta* 22, 977.
- (37) Ho F C, Ord J L (1972): *J Electrochem Soc* 119, 139.
- (38) Hoar P T, Yahalom J (1963): *J Electrochem Soc* 110, 614.
- (39) Hunter M S, Fowle P E (1954): *J Electrochem Soc* 101, 481.
- (40) JANAF (1971): Thermochemical tables, 2nd edn.
- (41) Johnson W K (1971): *Br Corros J* 6, 200.
- (42) Kaesche H (1960): *Z physik Chem NF* 26, 138.
- (43) Kaesche H (1962): *Z physik Chem NFF* 34, 87.
- (44) Kabanov B (1971): *Electrochim Acta* 16, 1321.
- (45) Kato M (1976): *Electrochim Acta* 21, 593.
- (46) Kohl P, Schultze J W (1973): *Z Electrochem Ber Bunsenges physik Chem* 77, 953.
- (47) Kunze J (1967): *Corros Sci* 7, 273.
- (48) Laser D, Yaniv M, Gottesfeld S (1978): *J Electrochem Soc* 125, 358.
- (49) Legault R A, Bettin W J (1971): *Mat Prot* 10, 3, 9.
- (50) Libsch T A, Devereux O F (1974): *J Electrochem Soc* 121, 400.

- (51) Libsch T A, Devereux O F (1974): *J Electrochem Soc* 123, 864.
- (52) McMullen J J, Pryor M J (1961): 1st International Congress on Metallic Corrosion, London.
- (53) Möller F, Memming R (1972): *Ber Bunsenges physik Chem* 76, 469.
- (54) Nagayama M, Cohen M (1962): *J Electrochem Soc* 109, 781.
- (55) Nisancioglu K, Holtan H (1975): 7th Scandinavian Corrosion Congress, Trondheim.
- (56) Nisancioglu K, Holtan H (1978): 8th Scandinavian Corrosion Congress, Helsinki.
- (57) Nisancioglu K, Holtan H (1979): *Electrochim Acta* 24, 1229.
- (58) Ogura K, Hackerman N (1972): *Electrochim Acta* 17, 1717.
- (59) Ord J L, Clayton J C, Wang W P (1977): *J Electrochem Soc* 124, 1671.
- (60) O'Sullivan J P, Wood G C (1970): *Proc Roy Soc A* 317, 511.
- (61) Pettinger B, Schöppel H R, Yokoyama T, Gerisher H (1974): *Z Electrochem Ber Bunsenges physik Chem* 78, 1024.
- (62) Rabbo M F, Richardson J A, Wood G C (1977): *Electrochim Acta* 22, 1375.
- (63) Reding J T, Newport J J (1966): *Mat Prot* 5, 12, 15.
- (64) Sato N, Kudo K, Nada T (1975): *Z physik Chem NF* 98, 271.
- (65) Sato N, Ohsuka T (1978): *J Electrochem Soc* 125, 1735.
- (66) Schmickler W (1978): *Z Electrochem Ber Bunsenges physik Chem* 82, 477.
- (67) Schultze J W, Stimming U (1975): *Z für physik Chem NF* 98, 285.
- (68) Schwabe K, Quy N (1963): *Monatsberichte Deutscher Akad Wiss Berlin* 5, 372.
- (69) Smith A W (1959): *Can J Phys* 37, 591.
- (70) Stimming U, Schultze J W (1976): *Ber Bunsenges physik Chem* 80, 1297.
- (71) Straumanis M E, Brakš N (1949): *J Electrochem Soc* 96, 310.
- (72) Tajma S (1977): *Electrochim Acta* 22, 995.
- (73) Taylor D F, Dignam M J (1973): *J Electrochem Soc* 120, 1299.
- (74) Towler C, Collins R A, Dearaley G (1975): *J Vac Sci Technol* 12, 520.
- (75) van Geel W Ch, Schelen B J J (1957): *Philips Research Repts* 12, 240.
- (76) Vermilyea D A (1954): *J Electrochem Soc* 101, 389.

- (77) Vermilyea D A (1957): *J Electrochem Soc* 104, 427.
- (78) Vermilyea D A (1957): *J Electrochem Soc* 104, 427.
- (79) Verwey E J W (1935): *Z Kristallogr (A)* 91, 315.
- (80) Verwey E J W (1935): *Physica* 2, 1059.
- (81) Vetter K J (1961): *Elektrochemische Kinetik* Springer-Verlag, Berlin-Göttingen-Heidelberg, 329.
- (82) Vetter K J (1955): *Elektrochem Ber Bunsenges physik Chem* 59, 67.
- (83) Vetter K J (1971): *Elektrochim Acta* 16, 1923.
- (84) Vetter K J (1962): *Z Elektrochem Ber Bunsenges physik Chem* 66, 577.
- (85) Vetter K J (1962): *J Electrochem Soc* 110, 597.
- (86) Vetter K J, Gorn F (1970): *Werkstoffe u Korrosion* 21, 703.
- (87) Vetter K J, Schultze J W (1973): *Z Elektrochem Ber Bunsenges physik Chem* 77, 945.
- (88) Videm K (1974): Kjeller Report KR-149, Institutt for Atomenergi.
- (89) Vielstich W, Schmickler W (1976): *Elektrochemie II: Kinetik elektrochemischer Systeme*, Steinkopff Darmstadt, 101.
- (90) Våland, T (1976): *Corros Sci* 16, 591.
- (91) Våland T, Heusler K E: To be published.
- (92) Wagner C (1973): *Ber Bunsenges physik Chem* 77, 1090.
- (93) Young I. (1957): *Trans Faraday Soc* 53, 841.
- (94) Young I. (1961): *Proc Royal Soc Ser A* 263, 395.

LIST OF SYMBOLS

$a_{Al^{3+}}$	activity of Al^{3+} in the oxide surface
$a_{O^{2-}}$	activity of O^{2-} in the oxide surface
a_{H^+}	activity of H^+ in the electrolyte
$A=j_0$	preexponential constant in the equation of anodization
$A(E)$	potential dependent term in the tunnelling equation (independent on the oxide thickness)
β	constant in the equation of anodization
B_j, B_r	constants in Dignam's equation of ion transport in oxides
cd	current density
C	electrical capacity
e	elementary charge
E	electrode potential
$E(0)$	electrode potential when there is no electric field in the oxide
$E_{1,2}$	potential difference between the metal and the oxide
E_2	potential difference across the oxide
$E_{2,3}$	potential difference across the oxide electrolyte interface
E_c	energy level corresponding to the bottom of the conduction band
E_F	energy of the Fermi level
E_F	anodizing voltage
E_j	electrode potential at constant current density
E_{stab}	electrode potential at steady state
ΔE	change in electrode potential during a potential step
ΔE_b^0	mean energy barrier height in the oxide when no field is present
$\Delta E_b(E)$	mean energy barrier height in the oxide

f	fraction of donors that are ionized in the bulk of the oxide
F	Faraday constant
ΔG_x^0	Gibbs free enthalpy
h	Planck constant
j	current density
j_a	anodic current density
j_c	Al dissolution rate
j_{ca}	charging current density
j_e	electronic current density
j_i	ionic current density
$j_0=A$	preexponential constant in the equation of anodization
j_{ox}	rate of oxide formation
k	Boltzmann constant
m_e	effective mass of electron
N_c	effective density of states
N_D	donor concentration in the oxide
N_D^0	donor concentration in the oxide surface towards the electrolyte when no space charge is present
pd	potential difference
q	constant in Dignam's equation of ion transport
q_{sc}	charge of the total space charge layer
R	series resistance
R	gas constant
R	time dependent parameter in Dignam's equation of ion transport
SCE	saturated calomel electrode
SHE	standard hydrogen electrode
t	time

T	absolute temperature
U	anodization ratio $\approx 14 \text{ \AA/V}$
V	electric field across the oxide
x	distance
$x_X()$	mole fraction
y	reaction order of H^+ in the oxide formation reaction
z	reaction order of H^+ in the metal dissolution reaction
α	constant in Young's equation of anodization
α	charge transfer coefficient
β	constant in Young's equation of anodization
β	effective transfer coefficient for the oxide formation
γ	effective transfer coefficient of the Al dissolution
δ	oxide thickness
δ_0	potential dependent term in the tunnelling equation (independent of the oxide thickness)
ϵ	relative dielectric constant of the oxide
ϵ_0	permittivity in vacuum
$\eta_{2,3}$	overvoltage at the oxide-electrolyte interphase
$\mu_X()$	chemical potential
$\mu_X^0()$	chemical potential in standard state
$\mu_X'(\text{ox})$	chemical potential of a specie in the oxide surface towards the metal
$\mu_X''(\text{ox})$	chemical potential of a specie in the oxide surface towards the electrolyte
$\mu_X(\text{ox})_0$	chemical potential of a specie in the equilibrium oxide
$\rho(x)$	space charge density as a function of distance
ρ_s	charge density in the oxide surface towards the electrolyte
$\varphi()$	electric potential

$\phi(\text{ox})$	potential of the oxide surface towards the metal
$\phi''(\text{ox})$	potential of the oxide surface towards the electrolyte
$\phi(\text{ox})_0$	potential of the equilibrium oxide
ϕ_s	potential of the oxide surface
$\Delta\phi_r$	potential difference across the reference electrode

DATE
ILME